
This item was submitted to [Loughborough's Research Repository](#) by the author.
Items in Figshare are protected by copyright, with all rights reserved, unless otherwise indicated.

Long-term dynamics driven by resonant wave-particle interactions: from Hamiltonian resonance theory to phase space mapping

PLEASE CITE THE PUBLISHED VERSION

<https://doi.org/10.1017/S0022377821000246>

PUBLISHER

Cambridge University Press (CUP)

VERSION

AM (Accepted Manuscript)

PUBLISHER STATEMENT

This article has been published in a revised form in *Journal of Plasma Physics*
<https://doi.org/10.1017/S0022377821000246>. This version is published under a Creative Commons CC-BY-NC-ND. No commercial re-distribution or re-use allowed. Derivative works cannot be distributed. © The Authors.

LICENCE

CC BY-NC-ND 4.0

REPOSITORY RECORD

Artemyev, Anton, Anatoly Neishtadt, Alexey Vasiliev, Xiao-Jia Zhang, Didier Mourenas, and Dmitri Vainchtein. 2021. "Long-term Dynamics Driven by Resonant Wave-particle Interactions: From Hamiltonian Resonance Theory to Phase Space Mapping". Loughborough University. <https://hdl.handle.net/2134/14043773.v1>.

Long-term dynamics driven by resonant wave-particle interactions: from Hamiltonian resonance theory to phase space mapping

Anton V. Artemyev^{1,2,†}, Anatoly I. Neishtadt^{3,2}, Alexei. A. Vasiliev²,
Xiao-Jia Zhang¹, Didier Mourenas⁴ and Dmitri Vainchtein^{5,2}

¹Institute of Geophysics and Planetary Physics, UCLA, Los Angeles, California 90095, USA;

²Space Research Institute of the Russian Academy of Sciences (IKI), 84/32 Profsoyuznaya Str., Moscow 117997, Russia;

³Department of Mathematical Sciences, Loughborough University, Loughborough LE11 3TU, United Kingdom;

⁴Laboratoire Matière sous Conditions Extrêmes, Paris-Saclay University, CEA, Bruyères-le-Châtel, France;

⁵Nyheim Plasma Institute, Drexel University, Camden, NJ, USA;

(Received xx; revised xx; accepted xx)

In this study we consider the Hamiltonian approach for the construction of a map for a system with nonlinear resonant interaction, including phase trapping and phase bunching effects. We derive basic equations for a single resonant trajectory analysis and then generalize them into the map in the energy/pitch-angle space. The main advances of this approach are the possibility to consider effects of many resonances and to simulate the evolution of the resonant particle ensemble on long time ranges. For illustrative purposes we consider the system with resonant relativistic electrons and field-aligned whistler-mode waves. The simulation results show that the electron phase space density within the resonant region is flattened with reduction of gradients. This evolution is much faster than the predictions of quasi-linear theory. We discuss further applications of the proposed approach and possible ways for its generalization.

1. Introduction

The resonant wave-particle interaction is known to be one of the main drivers of dynamics of such space plasma systems as planetary radiation belts (e.g., Thorne 2010; Menetti *et al.* 2012), collisionless shock waves (e.g., Balikhin *et al.* 1997; Wilson *et al.* 2007, 2012; Wang *et al.* 2020), auroral acceleration region (e.g., Chaston *et al.* 2008; Watt & Rankin 2009; Mauk *et al.* 2017), and solar wind (e.g., Krafft & Volokitin 2016; Kuzichev *et al.* 2019; Tong *et al.* 2019; Yoon *et al.* 2019; Roberg-Clark *et al.* 2019). The classical quasi-linear theory (Vedenov *et al.* 1962; Drummond & Pines 1962) and its generalizations for inhomogeneous plasma systems (Ryutov 1969; Lyons & Williams 1984) describe well charged particle resonant interaction with low-amplitude broadband waves (Karpman 1974; Shapiro & Sagdeev 1997; Tao *et al.* 2012a; Camporeale & Zimbardo 2015; Allanson *et al.* 2020).

One of the important examples of application of the quasi-linear theory is the Earth radiation belt models that describe energetic electron acceleration and losses due to resonances with electromagnetic whistler-mode waves and electromagnetic ion cyclotron

† Email address for correspondence: aartemyev@igpp.ucla.edu

41 (EMIC) waves (see reviews Thorne *et al.* 2010; Shprits *et al.* 2008; Ni *et al.* 2016;
 42 Nishimura *et al.* 2010; Millan & Thorne 2007, and references therein). Moreover, the nat-
 43 ural inhomogeneity of the background magnetic field and plasma density in the radiation
 44 belts can significantly weaken the conditions of applicability of the quasi-linear theory
 45 (Solovev & Shkliar 1986; Albert 2001, 2010). However, this theory meets difficulties in
 46 describing resonances with sufficiently intense waves (Shapiro & Sagdeev 1997), when the
 47 nonlinear effects of phase trapping and phase bunching become important (Omura *et al.*
 48 1991; Shklyar & Matsumoto 2009; Albert *et al.* 2013; Artemyev *et al.* 2018*a*). Indeed,
 49 sufficiently intense whistler-mode waves are frequently observed in the radiation belts
 50 (Cattell *et al.* 2008; Wilson *et al.* 2011; Agapitov *et al.* 2014) and contribute significantly
 51 to wave statistics (Zhang *et al.* 2018, 2019; Tyler *et al.* 2019). Theoretically, phase
 52 trapping and bunching (also called nonlinear scattering) effects are responsible for fast
 53 acceleration (e.g., Demekhov *et al.* 2006, 2009; Omura *et al.* 2007; Hsieh & Omura 2017;
 54 Hsieh *et al.* 2020) and losses (e.g., Kubota *et al.* 2015; Kubota & Omura 2017; Grach
 55 & Demekhov 2020) of energetic electrons and for the generation of coherent whistler-
 56 mode waves (Demekhov 2011; Katoh 2014; Katoh & Omura 2016; Tao 2014; Omura
 57 *et al.* 2008, 2013; Nunn & Omura 2012). There are many observational evidences of such
 58 nonlinear resonant wave generation (Titova *et al.* 2003; Cully *et al.* 2011; Tao *et al.* 2012*b*;
 59 Mourenas *et al.* 2015) and of the related electron acceleration/losses (e.g., Foster *et al.*
 60 2014; Agapitov *et al.* 2015*b*; Mourenas *et al.* 2016*a*; Chen *et al.* 2020; Gan *et al.* 2020*b*).

61 The quasi-linear diffusion theory describes a sufficiently weak scattering in
 62 energy/pitch-angle space and operates with a Fokker-Planck diffusion equation for
 63 the charged particle distribution function (Andronov & Trakhtengerts 1964; Kennel
 64 & Engelmann 1966; Lerche 1968). In contrast to this description, the nonlinear phase
 65 trapping assumes a fast transport in energy/pitch-angle space (e.g., Artemyev *et al.*
 66 2014*a*; Furuya *et al.* 2008), when even a single resonant interaction changes significantly
 67 the electron's energy/pitch-angle (e.g., Albert *et al.* 2013; Artemyev *et al.* 2018*a*). This
 68 essentially non-diffusive process cannot be directly included into the Fokker-Planck
 69 equation. One possible approach is the construction of an operator that would describe
 70 fast charged particle jumps in the energy/pitch-angle; this operator can be constructed
 71 with the numerical (test-particle) approach (e.g., Hsieh & Omura 2017; Zheng *et al.*
 72 2019) or with the analytical calculation of jumps' probabilities (e.g., Vainchtein *et al.*
 73 2018). The main advantage of this approach is the inclusion of almost arbitrary (as
 74 realistic as needed) wave spectrum and characteristics (e.g., wave modulation and
 75 frequency drifts, see Kubota & Omura 2018; Artemyev *et al.* 2019*b*; Hiraga & Omura
 76 2020). The main disadvantages are an accumulation of numerical errors with running
 77 time, and the almost intractable fine details of the energy/pitch-angle space binning
 78 needed to simultaneously resolve large jumps due to trapping and small changes due to
 79 drift/diffusion.

80 An alternative approach to the construction of such an operator is a generalization
 81 of the Fokker-Planck equation to include effects of phase trapping and phase bunching
 82 (Solovev & Shkliar 1986; Artemyev *et al.* 2016*b*, 2017). This approach is based on a
 83 fine balance of trappings and bunchings for a single wave system (e.g., Shklyar 2011;
 84 Artemyev *et al.* 2019*a*). The main advantage of this approach is that the evolution of
 85 charged particle distribution function can be investigated in arbitrary details in presence
 86 of phase trapping, phase bunching, and diffusion (Artemyev *et al.* 2018*b*, 2019*a*, e.g.,).
 87 The main disadvantage is that there is no straightforward generalization of this approach
 88 for multi-wave (multi-resonance) systems. A single-wave resonance results in charged
 89 particle transport in the energy/pitch-angle space along 1D curves, so-called resonance

90 surface curves (e.g., Lyons & Williams 1984; Summers *et al.* 1998), and the Fokker-Planck
 91 equation with trapping was derived for such a quasi-1D system (Artemyev *et al.* 2016*b*).

92 Another alternative for the description of charged particle distribution evolution driven
 93 by nonlinear wave-particle interaction (phase trapping and bunching) is the mapping
 94 technique that describes the characteristics of the Fokker-Planck equation (Van Kampen
 95 2003). The classical example of this approach is the Chirikov map (Chirikov 1979), which
 96 describes particle diffusion and is widely used for systems with wave-particle resonances
 97 (e.g., Vasilev *et al.* 1988; Zaslavskii *et al.* 1989; Benkadda *et al.* 1996; Khazanov *et al.*
 98 2013, 2014). Such a map has been constructed for a single-wave system with phase-
 99 trapping and phase bunching effects (Artemyev *et al.* 2020*b*). In this study we show the
 100 generalization of this map for a multi-resonance system.

101 We consider a strong magnetic field system, where charged particle motion is well
 102 gyrotopic and magnetic moments are well conserved away from the resonances. Thus,
 103 3D velocity space can be reduced to 2D energy/pitch-angle space. The mapping for
 104 this space should describe 2D charged particle motion due to energy/pitch-angle jumps
 105 with the time-intervals between jumps equal to the interval between passages through
 106 the resonances. Diffusive jumps (with zero mean values) and jumps driven by nonlinear
 107 phase bunching and phase trapping depend on the resonant phase φ_R , i.e. a variable
 108 proportional to the particle gyrophase, which changes fast. In low wave intensity systems
 109 this phase is randomly distributed over entire ($\varphi_R \in [0, 2\pi]$) range, and the phase
 110 dependence $\sim \sin \varphi_R$ can be directly included into the map (Vasilev *et al.* 1988; Zaslavskii
 111 *et al.* 1989; Benkadda *et al.* 1996; Khazanov *et al.* 2013, 2014). The phase bunching
 112 and phase trapping operate in certain φ_R ranges (e.g., Albert 1993; Itin *et al.* 2000;
 113 Grach & Demekhov 2020), whereas jumps depend on φ_R quite nonmonotonically (see
 114 Artemyev *et al.* (2014*b*, 2018*a*)). However, due to phase randomization between two
 115 successive resonances (see Appendix in (Artemyev *et al.* 2020*b*)), the phase-dependence
 116 can be reduced to a simplified determination of ranges corresponding to phase trapping
 117 $\varphi_R \in [0, 2\pi\Pi]$ and phase bunching $\varphi_R \in [\Pi, 2\pi]$ where $\Pi < 1$ is the probability of
 118 trapping (see, e.g., Artemyev *et al.* (2018*a*)). The phase gain between two resonances
 119 is a large value depending on particle energy and pitch-angle, but this dependence can
 120 be omitted in the leading approximation (see discussion in Artemyev *et al.* (2020*b*)).
 121 Therefore, in this study we consider charged particle transport in the energy/pitch-
 122 angle space due to nonlinear resonant interaction under assumption of resonant phase
 123 randomization (limitations of this assumption have been studied in Artemyev *et al.*
 124 (2020*a*)).

125 The paper structure includes a description of the basic system properties and examples
 126 of multi-resonant systems observed in the Earths radiation belts (Sect. 1). We present
 127 three examples: with two whistler-mode waves providing two cyclotron resonances, with
 128 one oblique whistler-mode wave providing cyclotron and Landau resonances, and with one
 129 whistler-mode wave and one EMIC wave providing two different cyclotron resonances.
 130 Then we focus on the first example and construct the map for this system (Sect. 2).
 131 Theoretical results derived from this map are verified with test particle simulations. At
 132 the end of the paper we discuss the constructed map and possible extensions of the
 133 proposed approach (Sect. 3).

134 2. Basic system properties

135 The Hamiltonian of a relativistic charged particle (e.g., an electron with rest mass m_e
 136 and charge $-e$) moving in the 2D inhomogeneous magnetic field of the Earth dipole and
 137 interacting with electromagnetic waves (in the low amplitude limit with the wave energy

138 U_w much smaller than electron energy $\sim m_e c^2$, where c is the speed of light) can be
 139 written as (e.g., Albert *et al.* 2013; Artemyev *et al.* 2018b):

$$H = m_e c^2 \gamma + U_w(s, I_x) \sin(\phi \pm n\psi)$$

$$\gamma = \sqrt{1 + \frac{p_{\parallel}^2}{m_e^2 c^2} + \frac{2I_x \Omega_{ce}}{m_e c^2}}, \quad (2.1)$$

140 where two pairs of conjugate variables are (s, p_{\parallel}) (the field-aligned coordinate and
 141 momentum) and (ψ, I_x) (gyrophase and momentum $I_x = c\mu/e$; μ is the classical magnetic
 142 moment). The electron gyrofrequency $\Omega_{ce} = eB_0/m_e c$ is determined by the background
 143 magnetic field $B_0(s)$, given by, e.g., the reduced dipole model (Bell 1984). The sign \pm in
 144 front of ψ is determined by the wave polarization: + for whistler-mode waves interacting
 145 with electrons and – for EMIC waves interacting with electrons. The resonance number
 146 is $n = 0, \pm 1, \pm 2, \dots$. The wave vector $\mathbf{k} = (k_{\parallel}(\omega, s), k_{\perp}(\omega, s))$ is given by cold plasma
 147 dispersion equation (Stix 1962) for a constant wave frequency ω (i.e., $\partial\phi/\partial s = k_{\parallel}$,
 148 $\partial\phi/\partial t = \omega$). For a finite angle $\theta = \arctan(k_{\perp}/k_{\parallel})$ between the wave vector and the
 149 background magnetic field the wave amplitude in Hamiltonian (2.1) takes the form
 150 (Albert 1993; Tao & Bortnik 2010; Nunn & Omura 2015; Artemyev *et al.* 2018b):

$$U_w = \sqrt{\frac{2I_x \Omega_{ce}}{m_e c^2}} \frac{eB_w}{k} \sum_{\pm} \frac{\cos\theta \pm C_1}{2\gamma} J_{n\pm 1} \left(\sqrt{\frac{2I_x k^2}{m_e \Omega_{ce}}} \sin\theta \right)$$

$$+ \frac{eB_w}{k} \left(\frac{p_{\parallel}}{\gamma m_e c} + C_2 \right) J_n \left(\sqrt{\frac{2I_x k^2}{m_e \Omega_{ce}}} \sin\theta \right) \sin\theta \quad (2.2)$$

151 where B_w is the wave magnetic field amplitude, $C_{1,2}$ are functions of wave dispersion
 152 and θ , and J_n are Bessel functions. Equation (2.2) shows that for field-aligned waves
 153 $\theta = 0$ there is only one cyclotron resonance $n = -1$: $U_w = \sqrt{2I_x \Omega_{ce}/m_e c^2} eB_w/k\gamma$ (with
 154 $C_1 = 1$ for $\theta = 0$, see (Tao & Bortnik 2010)). For oblique wave propagation $\theta \neq 0$ the
 155 whole set of resonances with different values of n is present.

2.1. Field-aligned whistler waves

156 Let us start with the system of two field-aligned whistler waves with the Hamiltonian:

$$H = m_e c^2 \gamma + \sqrt{\frac{2I_x \Omega_{ce}}{m_e c^2}} \frac{e}{\gamma} \sum_{i=0,1} \frac{B_{w,i}}{k_i} \sin(\phi_i + \psi) \quad (2.3)$$

158 where $\partial\phi_i/\partial s = k_i = k_i(\omega_i, s)$ with the two different wave frequencies ω_i . Figure 1 shows
 159 an example of such system observations. THEMIS spacecraft measures waves within
 160 the whistler-mode frequency range ($f \in [0.1, 1]f_{ce}$; $f_{ce} = \Omega_{ce}/2\pi$): there are two clear
 161 maxima in the magnetic and electric field spectra at $f \sim f_{ce}/4$ and $f \sim 3f_{ce}/8$ (see
 162 panels (a) and (b)). Both waves propagate along the background magnetic field: panel
 163 (c) shows θ as a function of the frequency. These double-peak spectra are quite typical
 164 for whistler-mode waves in the inner magnetosphere (see, e.g., Meredith *et al.* 2007; Ma
 165 *et al.* 2017; Crabtree *et al.* 2017; Zhang *et al.* 2020b; He *et al.* 2020; Yu *et al.* 2020).

166 To study electron energy/pitch-angle variation in the system with Hamiltonian (2.3),
 167 we follow the standard procedure (Neishtadt & Vasiliev 2006; Neishtadt 2014) and
 168 introduce the wave phases as new canonical variables, $\varphi_i = \phi_i + \psi$, with the generating

169 function:

$$W = sP + \left(\int k_0(\tilde{s})d\tilde{s} - \omega_0 t + \psi \right) I_0 + \left(\int k_1(\tilde{s})d\tilde{s} - \omega_1 t + \psi \right) I_1 \quad (2.4)$$

170 This function gives new variables: $P = p - k_0 I_0 - k_1 I_1$, $S = s$ (we keep s notation),
 171 $I_x = I_0 + I_1$, and new Hamiltonian $H_I = H + \partial W / \partial t = H - \omega_0 I_0 - \omega_1 I_1$

$$H_I = -\omega_0 I_0 - \omega_1 I_1 + m_e c^2 \gamma + \sqrt{\frac{2(I_0 + I_1) \Omega_{ce}}{m_e c^2}} \frac{e}{\gamma} \sum_{i=0,1} \frac{B_{w,i}}{k_i} \sin \varphi_i \quad (2.5)$$

$$\gamma = \sqrt{1 + \frac{(P + k_0 I_0 + k_1 I_1)^2}{m_e^2 c^2} + \frac{2(I_0 + I_1) \Omega_{ce}}{m_e c^2}}$$

172 Hamiltonian H_I describes a conservative system ($H_I = \text{const}$; without loss of generality
 173 we take $H_I = 0$) with three degrees of freedom, i.e., with three pairs of conjugate variables
 174 (s, P) , (φ_0, I_0) , (φ_1, I_1) . The resonance $\dot{\varphi}_i = 0$ conditions give $I_0 = I_{0R}(s, P, I_1)$, $I_1 =$
 175 $I_{1R}(s, P, I_0)$ as solutions of equations $\omega_i = m_e c^2 \partial \gamma / \partial I_i = 0$. Thus, there are two resonant
 176 surfaces. If these surfaces cross (i.e., at the same s, P electron can have simultaneously
 177 $I_0 = I_{0R}$ and $I_1 = I_{1R}$), then electrons can simultaneously be in resonance with the two
 178 waves (Shklyar & Zimbaro 2014; Zaslavsky *et al.* 2008). This quite complicated system
 179 would require a separate consideration (Sagdeev *et al.* 1988; Lichtenberg & Lieberman
 180 1983). Hereafter, we focus instead on the simpler case of well-separated resonances, when
 181 resonant surfaces do not cross. Equations $I_0 = I_{0R}$ and $I_1 = I_{1R}$ together with the
 182 condition $H_I = 0$ determine two families of curves in in (s, P) plane; values I_0 and I_1 are
 183 parameters of these families. Thus, on the curve $I_0 = I_{0R}(s, P, I_1)$ there is no change of I_1 ,
 184 and on the curve $I_1 = I_{1R}(s, P, I_0)$ there is no change of I_0 . With constant I_1 (or I_0) the I_0
 185 (or I_1) variation is directly related to the variation of energy: $-\omega_0 I_0 - \omega_1 I_1 + m_e c^2 \gamma = 0$.
 186 Taking into account that $I_0 + I_1 = I_x = m_e c^2 (\gamma^2 - 1) \sin^2 \alpha_{eq} / 2$, we can plot resonance
 187 curves (e.g., Lyons & Williams 1984; Summers *et al.* 1998; Mourenas *et al.* 2012), along
 188 which I_i change, in the energy/pitch-angle space $(m_e c^2 (\gamma - 1), \alpha_{eq})$ (note that we use the
 189 equatorial pitch-angle α_{eq} defined at the minimum of $B_0(s)$ field, i.e., at the minimum
 190 of $\Omega_{ce}(s)$). Figure 1(d) shows these curves $m_e c^2 \gamma - \omega_i I_i = \text{const}$: each curve of I_0 change
 191 corresponds to a fixed value of I_1 , and vice versa. Electrons move along these curves with
 192 the time-step of the interval between resonances. Note between resonances both I_i and
 193 γ are conserved, and electrons are moving along adiabatic orbits without wave influence,
 194 i.e. energy and pitch-angle change only at the resonances.

195 Let us consider electron dynamics in the energy/pitch-angle space for the system with
 196 Hamiltonian (2.3). We numerically integrate Hamiltonian equations for systems with a
 197 single wave and with two waves. Figures 2(a,b) show electron motion in the energy/pitch-
 198 angle space due to the resonance with a single wave. Solid curves are resonant curves of
 199 $-\omega_0 I_0 - \omega_1 I_1 + m_e c^2 \gamma = \text{const}$ for the wave frequency ω_0 and for the wave frequency ω_1 .
 200 Electrons move along this curve due to phase bunching (small negative jumps of energy
 201 and pitch-angle; see bottom panels) and phase trapping (rare large positive jumps of
 202 energy and pitch-angle; see bottom panels). Conservation of $-\omega_0 I_0 - \omega_1 I_1 + m_e c^2 \gamma$ and
 203 one of the momenta (I_0 or I_1) makes electron dynamics 1D in the energy/pitch-angle
 204 space. However, this dynamics becomes 2D in the system with two waves, when both
 205 I_0 and I_1 change, see Fig. 2(c). The electron moves along resonance curves and jumps
 206 between these curves due to I_i jumps. There are still the same energy and pitch-angle
 207 jumps due to phase bunching and phase trapping (see bottom panels), but electron phase

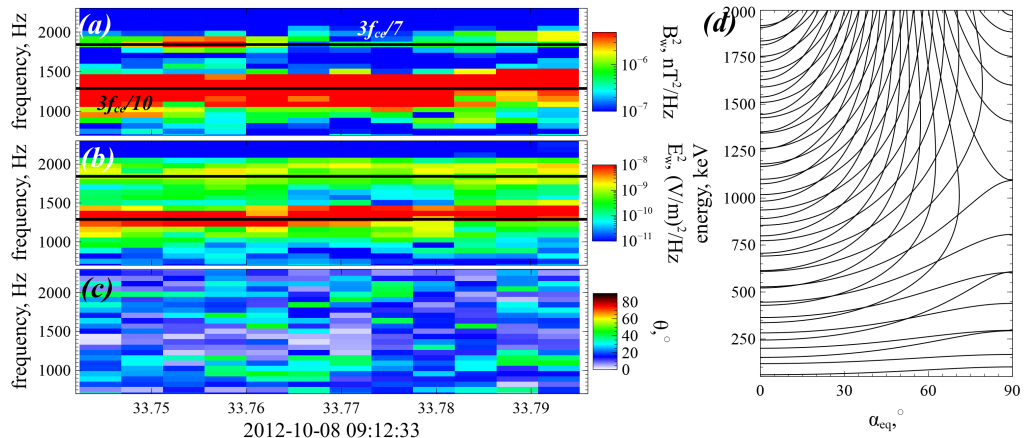


FIGURE 1. Observational example of two whistler-mode waves by Van Allen Probe A Mauk *et al.* (2013): magnetic field spectrum (a) and electric field spectrum (b) are obtained from EMFISIS measurements Kletzing *et al.* (2013), wave-normal angle (c) is estimated using the Mean's method Means (1972). Resonance curves for the system with two observed whistler-mode waves (d).

208 trajectory covers the entire energy/pitch-angle space. We describe this 2D dynamics with
 209 the mapping technique in this study.

210 2.2. Oblique whistler-mode wave

211 The second example corresponds to electron resonant interaction with a single oblique
 212 ($\theta \neq 0$) wave, for which Hamiltonian (2.1) takes the form

$$\begin{aligned}
 H &= m_e c^2 \gamma + \frac{eB_w}{k\gamma} h_0 \sin(\phi) + \sqrt{\frac{2I_x \Omega_{ce}}{m_e c^2}} h_1 \frac{eB_w}{k\gamma} \sin(\phi + \psi) \\
 h_0 &= -\sqrt{\frac{2I_x \Omega_{ce}}{m_e c^2}} C_1 J_1 + \left(\frac{p_{\parallel}}{m_e c} + C_2 \right) J_0 \sin \theta \\
 h_1 &= \frac{1}{2} (J_2(\cos \theta + C_1) + J_0(\cos \theta - C_1)) + \left(\frac{p_{\parallel}}{m_e c} + C_2 \right) \frac{kc}{2\Omega_{ce}} (J_2 + J_0) \sin \theta
 \end{aligned} \tag{2.6}$$

213 where we restrict our consideration to the first two resonances: Landau resonance
 214 $n = 0$ and the first cyclotron resonance $n = 1$. The Bessel function argument is
 215 $\sqrt{2I_x k^2 / m_e \Omega_{ce}} \sin \theta$. Such oblique whistler-mode waves are widely observed in the
 216 radiation belts (Agapitov *et al.* 2013, 2015a; Li *et al.* 2016), and their amplitudes are
 217 often sufficiently high for nonlinear resonances (Agapitov *et al.* 2015b; Artemyev *et al.*
 218 2016a; Mourenas *et al.* 2016a). Figure 3 shows an example of oblique whistler-mode wave
 219 measured by THEMIS spacecraft in the outer radiation belt. Electric and magnetic field
 220 spectra show the one wave power maximum around $f/f_{ce} \sim 1/3$ (see panels (a)&(b)),
 221 i.e. this is a single wave. Wave normal angle $\theta \approx 70^\circ$ (see panel (c)), i.e., this wave
 222 propagates obliquely to the background magnetic field.

223 Using the same approach as the one we applied for Hamiltonian (2.3), we introduce
 224 wave phases as new variables, $\varphi_0 = \phi_0$ and $\varphi_1 = \phi_1 + \psi$, using the generating function
 225 (Neishtadt & Vasiliev 2006; Neishtadt 2014):

$$W = sP + \left(\int k(\tilde{s}) d\tilde{s} - \omega t \right) I_0 + \left(\int k(\tilde{s}) d\tilde{s} - \omega t + \psi \right) I_1 \tag{2.7}$$

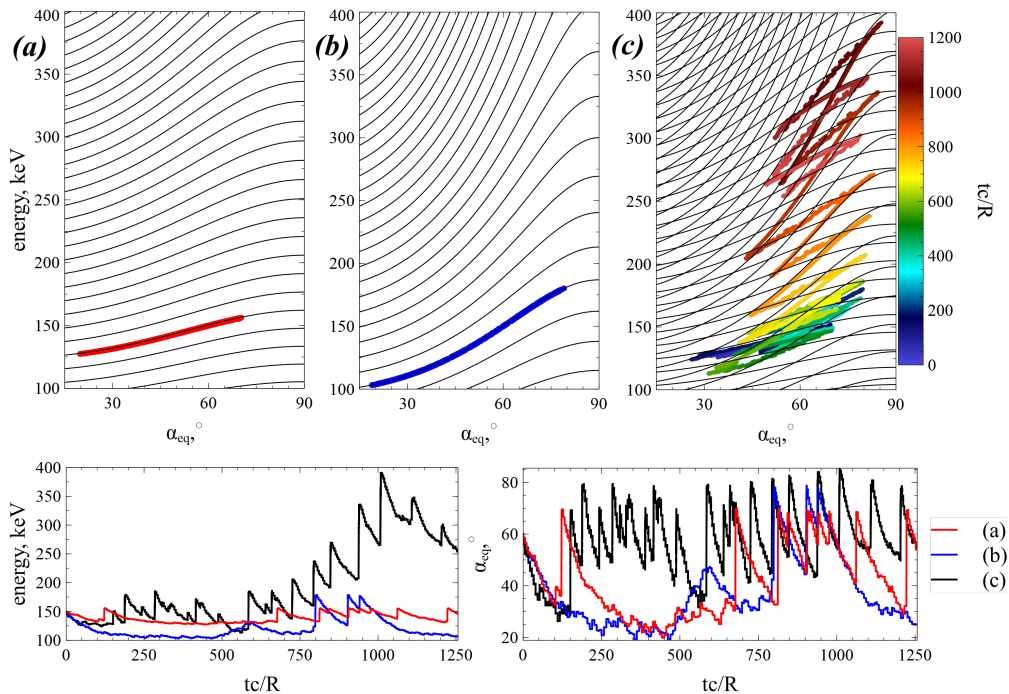


FIGURE 2. Top panels show resonance curves (black) and electron trajectories in the energy/pitch-angle space for Hamiltonian (2.3): only the first whistler-mode wave (a), only the second whistler-mode wave (b), both whistler-mode waves (c). In panel (c) different colors correspond to different time intervals. The bottom panels show energy and pitch-angle time series for the three trajectories in the top panels. We use parameters of dipole field at a radial distance of ~ 5 Earth radii. Plasma density is given by the model from Sheeley *et al.* (2001) and constant along magnetic field lines. Wave frequencies are $\omega_0 = 0.4\Omega_{ce}$, $\omega_1 = 0.2\Omega_{ce}$. Both wave amplitudes are 300 pT (see discussion of such wave observations in Zhang *et al.* 2018; Tyler *et al.* 2019). Wave amplitude is distributed along magnetic field line as $\tanh((\lambda/\delta\lambda_1)^2) \exp(-(\lambda/\delta\lambda_2)^2)$ with λ the magnetic latitude ($ds = R d\lambda \sqrt{1 + \sin^2 \lambda} \cos \lambda$) and $\delta\lambda_1 = 2^\circ$, $\delta\lambda_2 = 20^\circ$. This function fits the observed whistler-mode wave intensity distribution Agapitov *et al.* (2013).

226 This function gives the new variables: $P = p - k_0 I_0 - k_1 I_1$, $S = s$ (we keep s notation),
 227 $I_x = I_1$, and new Hamiltonian $H_I = H + \partial W / \partial t = H - \omega I_0 - \omega I_1$

$$H_I = -\omega I_0 - \omega I_1 + m_e c^2 \gamma + \frac{e B_w h_0}{k \gamma} \sin \varphi_0 + \sqrt{\frac{2 I_1 \Omega_{ce}}{m_e c^2}} \frac{e B_w h_1}{k \gamma} \sin \varphi_1 \quad (2.8)$$

$$\gamma = \sqrt{1 + \frac{(P + k_0 I_0 + k_1 I_1)^2}{m_e^2 c^2} + \frac{2 I_1 \Omega_{ce}}{m_e c^2}}$$

228 The resonance curves in the energy/pitch-angle space are given by two equations: $m_e c^2 \gamma -$
 229 $\omega I_1 = \text{const}$ with $I_1 = I_x = (\gamma^2 - 1) \sin^2 \alpha_{eq} / 2$ for the cyclotron resonance, and $I_x =$
 230 const for the Landau resonance. Figure 3(d) shows that at $\alpha_{eq} < \pi/4$ Landau resonance
 231 curves cross cyclotron resonance curves almost transversely, i.e., in the Landau resonance
 232 electrons quickly change energy with weaker pitch-angle change, whereas in the cyclotron
 233 resonance the energy change is more effective than the pitch-angle change.

234 To demonstrate the effects of the two resonances on electron transport in energy/pitch-
 235 angle space, we numerically integrate Hamiltonian equations (2.8) for three systems.
 236 Figure 4(a) shows results of the Landau resonance of the electron and oblique whistler-

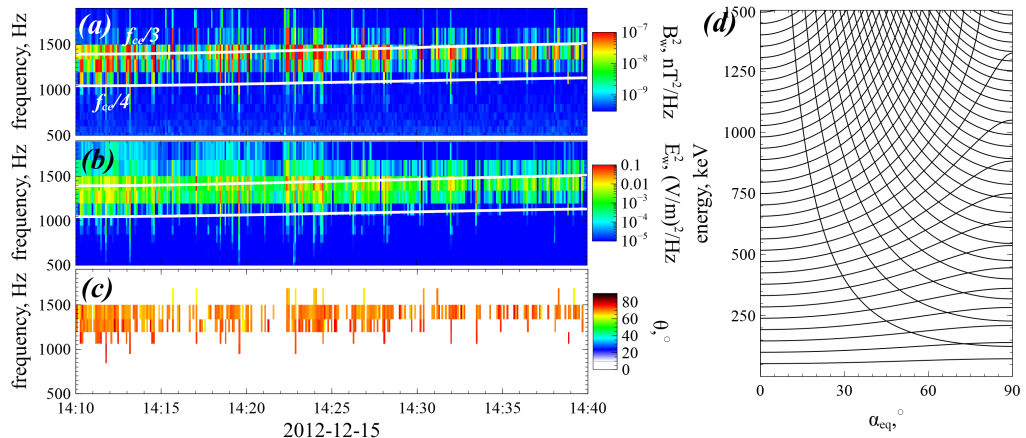


FIGURE 3. Observational example of oblique whistler-mode wave by Van Allen Probe A Mauk *et al.* (2013): magnetic field spectrum (a) and electric field spectrum (b) are obtained from EMFISIS measurements Kletzing *et al.* (2013), wave-normal angle (c) is estimated using the Mean's method Means (1972). Resonance curves for the system with two observed whistler-mode waves (d).

mode wave. The electron moves along a single resonant curve $I_x = rmconst$ with phase bunching responsible for pitch-angle increase and energy decrease, and the phase trapping responsible for pitch-angle decrease and energy increase (bottom panels). Figure 4(b) shows results of the cyclotron resonance: electron motion in the energy/pitch-angle space are quite similar to motions shown in Figs. 2(a&b): phase bunching is responsible for pitch-angle and energy decrease, whereas the phase trapping is responsible for pitch-angle and energy increase (bottom panels). The combination of the two resonances results in rapid electron motion within the whole energy/pitch-angle domain, see Fig. 4(c). The phase bunching decreases electron energy in both resonances, but moves electron in opposite directions in pitch-angle. As a result, a resonant electron loses energy until it reaches the region with high probability of trapping into the Landau resonance (Artemyev *et al.* 2013). After being trapped in Landau resonance, the electron gains energy and reaches the energy/pitch-angle domain where it can now be trapped into the cyclotron resonance with further energy increase. Such cycles of bunching, Landau trapping, and cyclotron trapping, quickly cover a large energy/pitch-angle domain for a single electron trajectory.

2.3. Field-aligned whistler-mode and EMIC waves

A third example is a system with field-aligned whistler-mode wave and field-aligned EMIC wave with polarization opposite to the whistler-mode wave. The corresponding Hamiltonian of a relativistic electron (reduction of Hamiltonian (2.2)) takes the form

$$H = m_e c^2 \gamma + \sqrt{\frac{2I_x \Omega_{ce}}{m_e c^2}} \left(\frac{eB_{w,0}}{k_0 \gamma} \sin(\phi_0 + \psi) + \frac{eB_{w,1}}{k_1 \gamma} \sin(\phi_1 - \psi) \right) \quad (2.9)$$

where $k_0 = k_0(\omega_0, s)$ follows the whistler-mode wave dispersion, whereas $k_1 = k_1(\omega_1, s)$ follows the EMIC wave dispersion. Figure 5(a&b) shows a typical example of observation of such two waves: the high-frequency magnetic field spectrum shows the whistler-mode wave with $f/f_{ce} \sim f_{ce}/2$, whereas the low-frequency magnetic field spectrum shows the EMIC wave with $f/f_{cp} \sim f_{cp}/2$ (f_{cp} is the proton gyrofrequency). The EMIC wave is field-aligned (see panel (c)). Due to the low EMIC wave frequency, the resonance

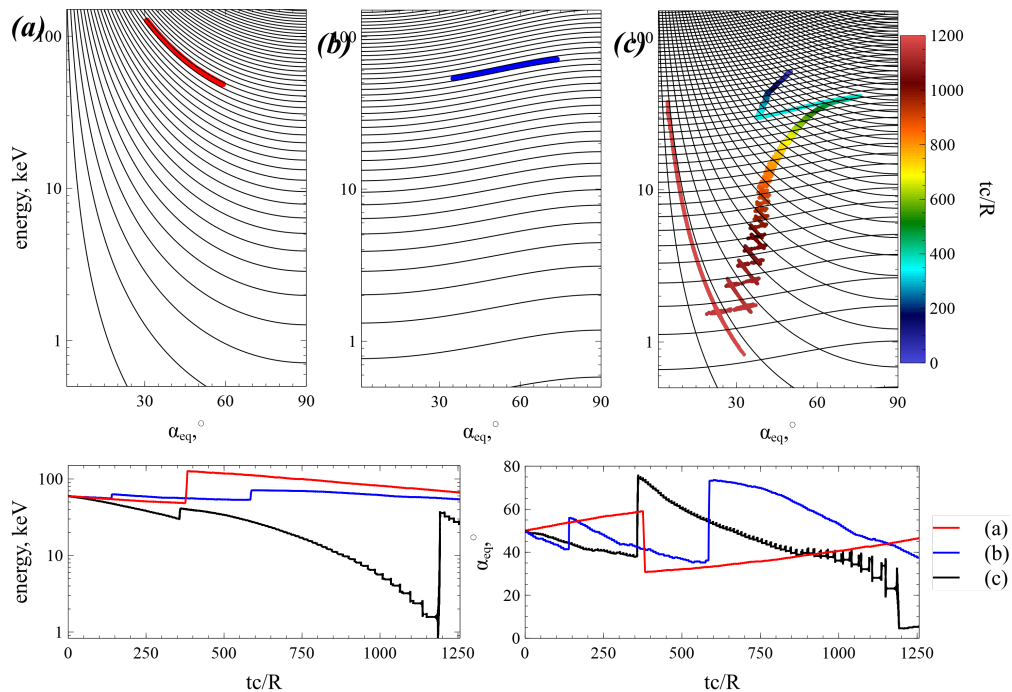


FIGURE 4. Top panels show resonance curves (black) and electron trajectories in the energy/pitch-angle space for Hamiltonian (2.6): only Landau resonance (a), only cyclotron resonance (b), both resonances (c). In panel (c) color shows time. Bottom panels show energy and pitch-angle time series for three trajectories from top panels. System parameters are the same as in Fig. 2, wave frequency is $\omega = 0.35\Omega_{ce}$, wave amplitude is 500 pT, and wave normal angle θ is 5° away of the resonance cone angle $\text{acos}(\omega/\Omega_{ce})$ (see discussion of such wave observations in Wilson *et al.* 2011; Agapitov *et al.* 2014; Artemyev *et al.* 2016a; Mourenas *et al.* 2016a). The wave amplitude distribution along magnetic field-lines is the same as one used in Fig. 1.

condition $\dot{\phi}_1 - \dot{\psi} = k_1 p / \gamma - \omega_1 - \Omega_{ce} / \gamma = 0$ can be reduced to $k_1 p = \Omega_{ce}$, with typical k_1 about the inverse ion inertial length (Silin *et al.* 2011). Thus, only high-energy electrons (with large enough p) can resonate with EMIC waves (e.g., in the Earth radiation belts the resonant energy is typically larger than ~ 1 MeV, see Thorne & Kennel (1971); Summers & Thorne (2003); Shprits *et al.* (2016); Chen *et al.* (2019)). Let us compare whistler-mode and EMIC wave resonance curves for such high energies.

First, we introduce wave phases as new variables, $\varphi_0 = \phi_0 + \psi$ and $\varphi_1 = \phi_1 - \psi$, with the generating function (Neishtadt & Vasiliev 2006; Neishtadt 2014):

$$W = sP + \left(\int k_0(\tilde{s})d\tilde{s} - \omega_0 t + \psi \right) I_0 + \left(\int k_1(\tilde{s})d\tilde{s} - \omega_1 t - \psi \right) I_1 \quad (2.10)$$

This function gives new variables: $P = p - k_0 I_0 - k_1 I_1$, $S = s$ (we keep s notation), $I_x = I_0 - I_1$, and new Hamiltonian $H_I = H + \partial W / \partial t = H - \omega I_0 - \omega I_1$

$$H_I = -\omega_1 I_0 - \omega_1 I_1 + m_e c^2 \gamma + \sqrt{\frac{2(I_0 - I_1)\Omega_{ce}}{m_e c^2}} \sum_{i=0,1} \frac{eB_{w,i}}{k_i \gamma} \sin \varphi_i$$

$$\gamma = \sqrt{1 + \frac{(P + k_0 I_0 + k_1 I_1)^2}{m_e^2 c^2} + \frac{2(I_0 - I_1)\Omega_{ce}}{m_e c^2}} \quad (2.11)$$

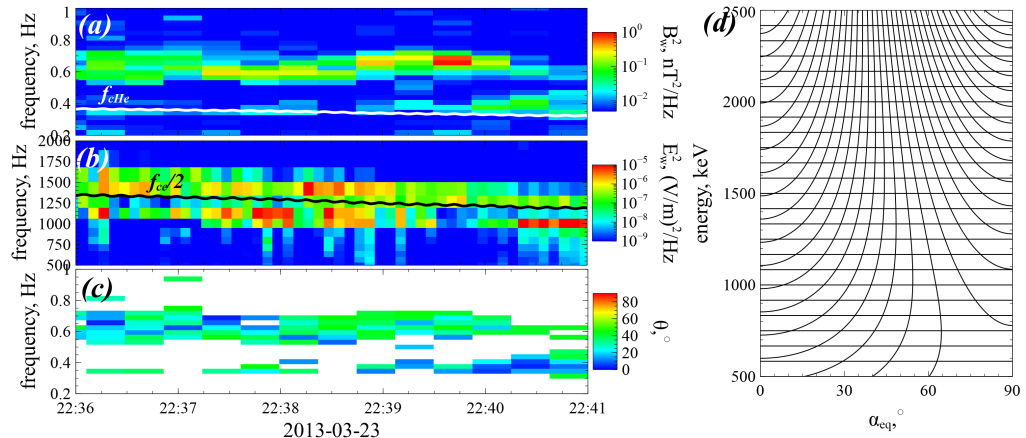


FIGURE 5. Observational example of a system with whistler-mode and EMIC waves by Van Allen Probe A Mauk *et al.* (2013): magnetic field spectrum of EMIC wave (a) and whistler-mode wave (b) are obtained from EMFISIS measurements Kletzing *et al.* (2013), the wave-normal angle of the EMIC wave (c) is estimated using the Mean’s method Means (1972). Resonance curves for the system with the two observed whistler-mode waves (d).

273 The EMIC resonance curves are given by equation $m_e c^2 \gamma - \omega_1 I_1 = \text{const}$, and taking
 274 into account the smallness of ω_1 we obtain $\gamma \approx 0$, i.e. resonance curves are almost
 275 straight lines parallel to the energy axis (see Fig. 5(d)). The whistler-mode resonance
 276 curves ($m_e c^2 \gamma - \omega_0 I_0 = \text{const}$ with $I_0 = I_x + \text{const}$) cross these lines: the EMIC wave is
 277 responsible for electron transport along pitch-angle space, and the whistler-mode wave
 278 leads to both pitch-angle and energy changes. Figure 6(a&b) confirms this scenario:
 279 the EMIC wave resonates with small pitch-angle (large p) electron and phase bunch
 280 it to larger pitch-angles (phase trapping by EMIC waves is responsible for pitch-angle
 281 decrease; see bottom panel) with an approximate conservation of energy, whereas the
 282 whistler-mode wave can resonate with large pitch-angle electrons and transport them to
 283 smaller pitch-angles via phase bunching with energy decrease (moving them away from
 284 the EMIC wave resonance).

285 The combination of EMIC and whistler-mode wave resonances (see Fig. 6(c)) can
 286 result in a very effective transport of large pitch-angle electrons to small pitch-angles
 287 (rapid electron losses): bunching of ~ 2 MeV electrons with initially large pitch-angles
 288 results in electron transfer to small pitch-angles, where even faster EMIC phase trapping
 289 may move this electron to the loss-cone (see discussions of similar effects of combined
 290 EMIC and whistler-mode waves in the diffusive approximation in (Mourenas *et al.* 2016b;
 291 Zhang *et al.* 2017)). From small pitch-angles (note that the loss-cone is not included in
 292 our simulations) the EMIC wave can transport an electron via phase bunching to higher
 293 pitch-angles, where whistler-mode resonance can accelerate it via trapping. As a result
 294 of so different resonant interactions with EMIC and whistler-mode waves, the electron
 295 trajectory can quickly fill up a large domain in the energy/pitch-angle space.

296 3. Mapping technique for multi-resonances

297 To describe the long-term evolution of electron dynamics in the energy/pitch-angle
 298 space, we propose to develop a map providing relations for each resonant interaction
 299 $\Delta\gamma = \Delta\gamma(\gamma, \alpha_{eq})$, $\Delta\alpha_{eq} = \Delta\alpha(\gamma, \alpha_{eq})$. Changes $\Delta\gamma, \Delta\alpha_{eq}$ are due to phase bunching
 300 (nonlinear scattering) and phase trapping. Thus, the first step in the construction of

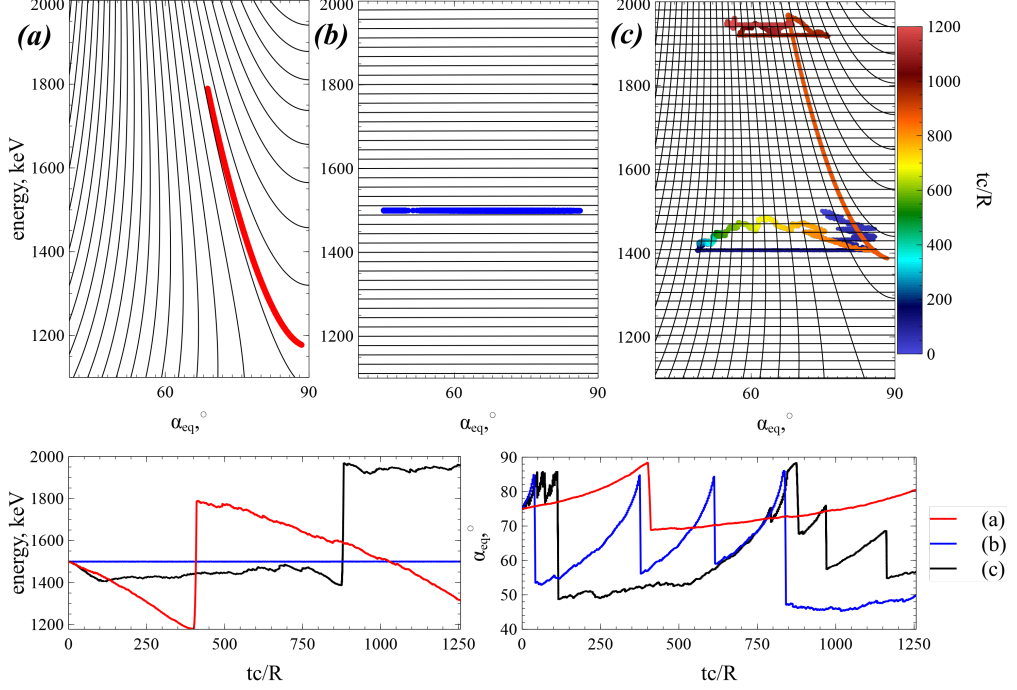


FIGURE 6. Top panels show resonance curves (black) and electron trajectories in the energy/pitch-angle space for Hamiltonian (2.9): only whistler-mode wave (a), only EMIC wave (b), both whistler-mode and EMIC waves (c). In panel (c) color shows time. Bottom panels show energy and pitch-angle time series for three trajectories in the top panels. System parameters are the same as in Fig. 2. EMIC wave is H^+ band with the frequency $\omega = 0.7\Omega_{cp}$ and amplitude 1 nT (see discussion of such wave observations in Zhang *et al.* 2016; Kersten *et al.* 2014). Whistler-mode wave frequency is $\omega = 0.35\Omega_{ce}$, and wave amplitude is 300 pT. The wave amplitude distribution along magnetic field-lines is the same as one used in Fig. 1.

301 such a map is to derive equations for $\Delta\gamma$, $\Delta\alpha_{eq}$ driven by both these processes. We start
 302 with Hamiltonian (2.5) and follow the standard procedure of Hamiltonian expansion
 303 around the resonant I_0, I_1 values (Neishtadt 2014; Artemyev *et al.* 2018a), which are
 304 defined by equations $\partial H_I / \partial I_i = 0$:

$$\frac{k_i I_{iR}}{m_e c} = -\frac{P + k_{i'} I_{i'}}{m_e c} - \frac{\Omega_{ce}}{k_i} + \frac{1}{\sqrt{(k_i c / \omega_i)^2 - 1}} \sqrt{1 - \left(\frac{\Omega_{ce}}{k_i c}\right)^2 - 2 \frac{\Omega_{ce}}{k_i c} \frac{P + (k_{i'} - k_i) I_{i'}}{m_e c}} \quad (3.1)$$

305 where $i = 0$ for $i = 1$ and $i = 1$ for $i = 0$. Expansion of Hamiltonian (2.5) around $I_i = I_{iR}$
 306 gives

$$\begin{aligned} H_{I_i} &\approx \Lambda_i + m_e c^2 \frac{1}{2} g_i (I_i - I_{iR})^2 + u_{iR} \sin \varphi_i \\ \Lambda_i &= m_e c^2 \gamma_{iR} - (\omega_0 I_0 + \omega_1 I_1)_{I_i=I_{iR}} \\ \gamma_{iR} &= \frac{(k_i c / \omega_i)}{\sqrt{(k_i c / \omega_i)^2 - 1}} \sqrt{1 - \left(\frac{\Omega_{ce}}{k_i c}\right)^2 - 2 \frac{\Omega_{ce}}{k_i c} \frac{P + (k_{i'} - k_i) I_{i'}}{m_e c}} \end{aligned} \quad (3.2)$$

$$u_{iR} = \sqrt{\frac{2\Omega_{ce}(I_0 + I_1)_{I_i=I_{iR}}}{m_e c^2}} \frac{e}{\gamma_{iR}} \frac{B_{w,i}}{k_i}$$

$$g_i = \left. \frac{\partial^2 \gamma}{\partial I_i^2} \right|_{I_i=I_{iR}} = \frac{k_i^2}{m_e^2 c^2}$$

307 where φ_i are fast variables and $I_i - I_{iR}$ and (s, P) are slow variables (note that Λ_i does
 308 not depend on fast variables). Next, we introduce new variables $P_{\varphi_i} = I_i - I_{iR}$ with the
 309 generating function $Q_i = (I_i - I_{iR})\varphi_i + s\tilde{P}_i$. New Hamiltonians are

$$F_i = \Lambda_i(\tilde{s}, \tilde{P}) + m_e c^2 \frac{1}{2} g_i P_{\varphi_i}^2 + u_{iR} \sin \varphi_i \quad (3.3)$$

$$\approx \Lambda_i(s, P) + \{\Lambda_i, I_{iR}\}_{s,P} \varphi_i + m_e c^2 \frac{1}{2} g_i P_{\varphi_i}^2 + u_{iR} \sin \varphi_i$$

310 where $\tilde{s} = s - (\partial I_{iR}/\partial P)\varphi_i$, $\tilde{P} = p + (\partial I_{iR}/\partial s)\varphi_i$, $\{\}$ are Poisson brackets, and we
 311 expand $\Lambda(\tilde{s}, \tilde{P})$ over small $\partial I_{iR}/\partial s$, $\partial I_{iR}/\partial P$ terms. Hamiltonian F_i is the sum of $\Lambda_i(s, P)$
 312 describing slow variable dynamics and pendulum Hamiltonian describing fast variable
 313 dynamics:

$$F_{\varphi_i} = m_e c^2 \frac{1}{2} g_i P_{\varphi_i}^2 + \{\Lambda_i, I_{iR}\}_{s,P} \varphi_i + u_{iR} \sin \varphi_i \quad (3.4)$$

314 where the coefficients depend on the slow variables. Figure 7 shows phase portraits of F_{φ_i}
 315 for systems with $a_i = |u_{iR}/\{\Lambda_i, I_{iR}\}| < 1$ (panel a) and with $a_i = |u_{iR}/\{\Lambda_i, I_{iR}\}| > 1$
 316 (panel b). For low wave amplitude $a_i < 1$ the phase portrait does not contain closed
 317 orbits, i.e., all particles cross the resonance $\dot{\varphi}_i = m_e c^2 g_i P_{\varphi_i} = 0$ within an interval of
 318 about one period of φ_i . There are only weak scatterings in this regime with zero mean
 319 changes of I_i , and such scatterings can be described by the quasi-linear diffusion model
 320 for inhomogeneous plasma (e.g., Karpman 1974; Albert 2010; Grach & Demekhov 2020).
 321 For sufficiently high wave amplitude $a_i > 1$, however, the phase portrait contains both
 322 closed and open orbits, i.e., there are now phase trapped particles oscillating around the
 323 resonance $\dot{\varphi}_i = m_e c^2 g_i P_{\varphi_i} = 0$ for a long time. Scattering (crossing of the resonance
 324 along the open orbits) would result in phase bunching with a small, yet nonzero mean
 325 change of I_i (see reviews by Shklyar & Matsumoto 2009; Albert *et al.* 2013, and references
 326 therein), whereas phase trapping would significantly change I_i . We would like to include
 327 this nonlinear regime of wave-particle interaction into the map in energy/pitch-angle
 328 space. For this reason, we derive expressions for changes of I_i due to phase bunching,
 329 $\Delta_{\text{scat}} I_i$, and due to phase trapping $\Delta_{\text{trap}} I_i$. As $\Delta_{\text{scat}} I_i$ is local, i.e. depends on particle
 330 and system characteristics at the resonance, we can keep slow variables unchanged for
 331 $\Delta_{\text{scat}} I_i$ evaluations:

$$\begin{aligned} \Delta_{\text{scat}} I_i &= 2 \int_{-\infty}^{t_{iR}} \frac{\partial H_{I_i}}{\partial I} dt = \frac{2u_{iR}}{m_e c^2 g_i} \int_{-\infty}^{\varphi_{iR}} \frac{\cos \varphi_i d\varphi_i}{P_{\varphi_i}} \\ &= \sqrt{\frac{2u_{iR}}{m_e c^2 g_i}} \int_{-\infty}^{\varphi_{iR}} \frac{\sqrt{u_{iR}} \cos \varphi_i d\varphi_i}{\sqrt{F_{\varphi_i} - \{\Lambda_i, I_{iR}\}_{s,P} \varphi_i - u_{iR} \sin \varphi_i}} \\ &= \sqrt{\frac{2u_{iR}}{m_e c^2 g_i}} \int_{-\infty}^{\varphi_{iR}} \frac{\sqrt{u_{iR}} \cos \varphi_i d\varphi_i}{\sqrt{\{\Lambda_i, I_{iR}\}_{s,P} (\varphi_{iR} - \varphi_i) + u_{iR} (\sin \varphi_{iR} - \sin \varphi_i)}} \end{aligned} \quad (3.5)$$

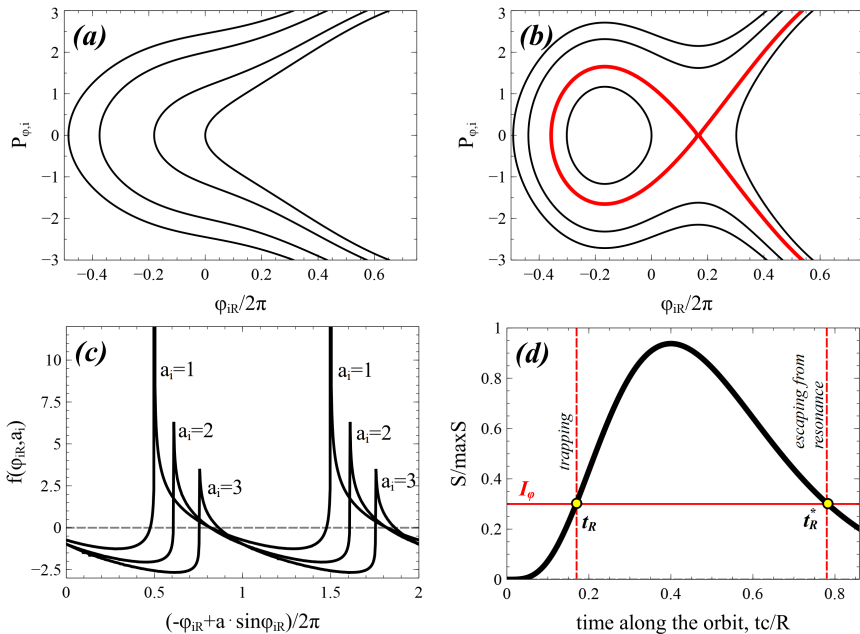


FIGURE 7. Phase portraits of F_{φ_i} for systems with $|u_{iR}| < |\{\Lambda_i, I_{iR}\}|$ (a) and with $|u_{iR}| > |\{\Lambda_i, I_{iR}\}|$ (b). Black curves show contours of $F_{\varphi_i} = \text{const}$, red curve is the separatrix demarcating region of trapped (closed) electrons orbits and region of transient (open) orbits. Function $f(h_\phi, a)$ for several a and $(-\varphi_{iR} + a \sin \varphi_{iR})/2\pi$ (c) and scheme of trapping/detrapping (d).

$$= \sqrt{\frac{2u_{iR}}{m_e c^2 g_i}} \int_{-\infty}^{\varphi_{iR}} \frac{\sqrt{a_i} \cos \varphi_i d\varphi_i}{\sqrt{(\varphi_{Ri} - \varphi_i) + a_i (\sin \varphi_{Ri} - \sin \varphi_i)}} = \sqrt{\frac{2u_{iR}}{m_e c^2 g_i}} f_i(\varphi_{Ri}, a_i)$$

332 where t_{iR} is the time of passage through the resonance, φ_{iR} is the wave phase at this time,
 333 and we use $\dot{\varphi}_i = m_e c^2 g_i P_{\varphi_i} = 2^{1/2} \sqrt{F_{\varphi_i} - \{\Lambda_i, I_{iR}\} \varphi_i - u_{Ri} \sin \varphi_i}$, $F_{\varphi_i} = \{\Lambda_i, I_{iR}\} \varphi_{Ri} +$
 334 $u_{Ri} \sin \varphi_{Ri}$ (resonant energy F_{φ_i} value evaluated at $P_{\varphi_i} = 0$). Note Eq. (3.5) describes
 335 $\Delta_{\text{scat}} I_i$ change for the particle motion through the resonance from $-\infty$ to resonant
 336 φ_{iR} , whereas the motion in opposite direction would result in change of sign of $\Delta_{\text{scat}} I_i$.
 337 Function $f_i(a_i, \varphi_{iR})$ is periodic for φ_{iR} , see Fig. 7(c). Although the sign of f_i changes
 338 within one φ_{iR} period, the mean value of this function for $a_i > 1$ is not zero, providing
 339 the effect of phase bunching. To consider the precise $\Delta_{\text{scat}} I_i$ dependence on φ_{iR} in the
 340 mapping, one would need to keep information about resonant phase φ_i and calculate
 341 the phase gain between resonances. However, the phase is fast rotating, and even a
 342 small change of φ_i at the resonance would result in a significant change of phase gain
 343 between resonances. Therefore, we can assume that φ_{iR} is a random variable with a
 344 uniform distribution of the resonant energy $F_{\varphi_i}(\varphi_{iR})$ at $P_{\varphi_i} = 0$ axis (see justification
 345 of this assumption in Itin *et al.* (2000); Artemyev *et al.* (2020a,b)), and all resonant
 346 particles with the same slow variables (same energy and pitch-angle) at the resonance
 347 would experience the same ΔI_i change equal to $\langle \Delta I_i \rangle$ averaged over the resonant energy
 348 (Artemyev *et al.* 2020b).

349 An important property of f function from Eq. (3.5) is that being averaged over energies

350 in resonance, $F_{\varphi_i} = \{A_i, I_{iR}\}\varphi_{Ri} + u_{Ri} \sin \varphi_{Ri}$, this function gives

$$\langle f_i \rangle = -\sqrt{\frac{m_e c^2 g_i}{2u_{iR}}} \frac{S}{2\pi} = -\sqrt{\frac{8|u_{iR}|}{a_i m_e c^2 g_i}} \int_{\varphi_{i-}}^{\varphi_{iR}} \sqrt{(\varphi_{Ri} - \varphi_i) + a_i (\sin \varphi_{Ri} - \sin \varphi_i)} d\varphi_i \quad (3.6)$$

351 where S is the area surrounded by the separatrix in the phase portrait in Fig. 7(b)
 352 (see details of Eq. (3.6) derivations in Neishtadt (1999) and Artemyev *et al.* (2018a)).
 353 Therefore, the $\Delta_{scat} I_i$ change due to phase bunching is equal to $-S/2\pi$ and for $a_i \gg$
 354 1 (i.e. for very weak magnetic field inhomogeneity; note $\{A_i, I_{iR}\} \sim \partial/\partial s$) we have
 355 $\Delta_{scat} I_i = -8\sqrt{2u_{iR}/m_e c^2 g_i}$ where $S = 16\sqrt{2u_{iR}/m_e c^2 g_i}$ is the width of the resonance
 356 for large amplitude waves (Palmadesso 1972; Karimabadi *et al.* 1990).

357 The change of I_i due to phase bunching (nonlinear scattering) is sufficiently small to
 358 consider this process locally in energy/pitch-angle space, i.e., $\Delta_{scat} I_i \ll I_i$ (see discussion
 359 of exceptions for $\Delta_{scat} I_i \sim I_i$ in Appendix A), whereas the change of I_i due to phase
 360 trapping is essentially non-local. To evaluate $\Delta_{trap} I_i$, we take into account that $I_i = I_{iR}$ in
 361 the resonance (during the trapping), the trapping time is defined as $2\pi I_\phi = \int P_{\varphi_i} d\varphi_{iR} =$
 362 S , and I_ϕ is conserved during the trapping (because trapped particles oscillate in the
 363 $(\varphi_{iR}, P_{\phi_i})$ plane much faster than the system evolves (much faster than variations of
 364 slow variables s, P). Thus, the trapping time is defined as the time of arrival to the
 365 resonance t_R with $\dot{S}(t_R) > 0$ (the growth of the area surrounded by the separatrix allows
 366 trapping of particles moving along open trajectories into closed trajectories), whereas
 367 the time t_R^* of escape from the trapping is defined by $S(t_R^*) = S(t_R)$ and $\dot{S}(t_R^*) < 0$ (see
 368 scheme in Fig. 7(d)):

$$\Delta_{trap} I_i = I_{iR}(t_{iR}^*) - I_{iR}(t_{iR}), \quad S(t_{iR}^*) = S(t_{iR}), \quad \dot{S}(t_{iR}) > 0, \quad \dot{S}(t_{iR}^*) < 0 \quad (3.7)$$

369 At the resonance, an electron can be scattered (i.e., experience the phase bunching) or
 370 trapped, and this depends on the φ_{iR} value (e.g., Albert 1993; Itin *et al.* 2000; Grach
 371 & Demekhov 2018). However, as φ_{iR} is a fast oscillating variable, we can consider the
 372 so-called probability of trapping instead of tracing the precise φ_{iR} value: the range of φ_{iR}
 373 of trapped particles, i.e., the ratio of trapped particles to the total number of resonant
 374 particles for a single resonance, is the probability of trapping, Π_i (e.g., Arnold *et al.* 2006,
 375 and references therein). For small Π_i , this probability is defined as the ratio of the change
 376 of the area under the separatrix, \dot{S} , and the total resonant flux $\int_0^{2\pi} \dot{P}_{\varphi_i} d\phi = 2\pi\{A_i, I_{iR}\}$:
 377 $\Pi_i = \dot{S}/2\pi\{A_i, I_{iR}\} = \{S, F_i\}/2\pi\{A_i, I_{iR}\}$. This definition of the trapping probability
 378 has been verified for various plasma systems (e.g., Artemyev *et al.* 2014b; Leoncini *et al.*
 379 2018; Vainchtein *et al.* 2018). Therefore, the resonant interaction can be characterized
 380 by Π , $\Delta_{trap} I_i$, and $\Delta_{scat} I_i$.

381 Due to conservation of $H_i = m_e c^2 \gamma - \omega_0 I_0 - \omega_1 I_1$, changes of I_i are directly related to
 382 γ changes, whereas the $I_x = I_0 + I_1$ relation gives the pitch-angle change:

$$\frac{\omega_i \sin^2 \alpha_{eq}}{\gamma^2 - 1} (\Delta_i \gamma)^2 - 2\Delta_i \gamma \frac{\Omega_{eq} - \gamma \omega_i \sin^2 \alpha_{eq}}{\gamma^2 - 1} + \omega_i (\sin^2(\alpha_{eq} + \Delta_i \alpha_{eq}) - \sin^2 \alpha_{eq}) = 0$$

383 that for small changes (phase bunching) can be rewritten as

$$\Delta_i \alpha_{eq} = \Delta_i \gamma \frac{\Omega_{eq} - \gamma \omega_i \sin^2 \alpha_{eq}}{\omega_i \sin \alpha_{eq} \cos \alpha_{eq} (\gamma^2 - 1)} \quad (3.8)$$

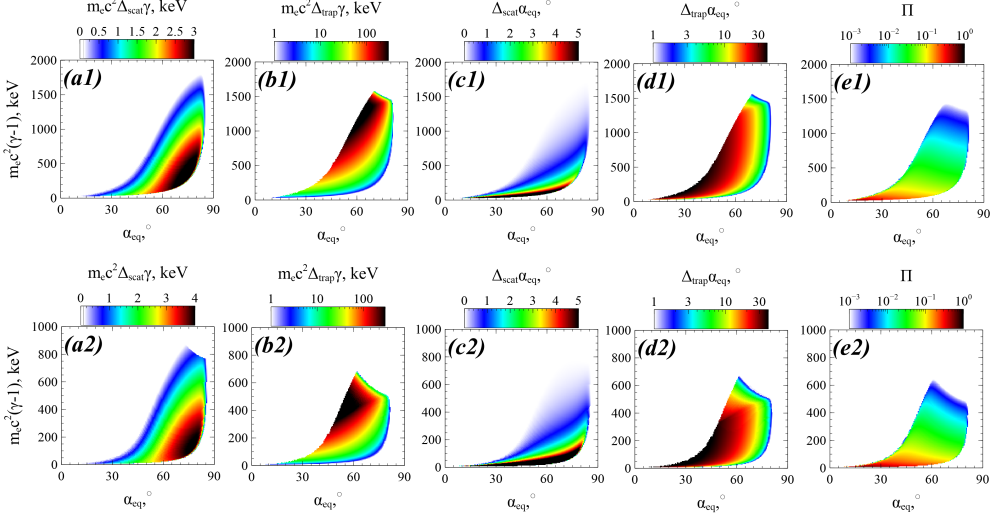


FIGURE 8. System characteristics for two field-aligned whistler-mode waves with the parameters as in Fig. 1: energy change due to scattering (a) and trapping (b), pitch-angle change due to scattering (c) and trapping (d), trapping probability (e).

384

Therefore, the map for one resonance can be written as

$$\begin{aligned}
 \begin{pmatrix} \bar{\gamma} \\ \bar{\alpha}_{eq} \end{pmatrix} &= \begin{pmatrix} G_{\gamma i}(\gamma, \alpha_{eq}) \\ G_{\alpha i}(\gamma, \alpha_{eq}) \end{pmatrix} = \begin{pmatrix} \gamma \\ \alpha_{eq} \end{pmatrix} + \begin{pmatrix} \Delta_i \gamma \\ \Delta_i \alpha_{eq} \end{pmatrix} \\
 \Delta_i \gamma &= \omega_i \begin{cases} \Delta_{scat} I_i(\gamma, \alpha_{eq}), & \xi_i \in [\Pi_i(\gamma, \alpha_{eq}), 1] \\ \Delta_{trap} I_i(\gamma, \alpha_{eq}), & \xi_i \in [0, \Pi_i(\gamma, \alpha_{eq})] \end{cases} \\
 \Delta_i \alpha_{eq} &= \begin{cases} \frac{\Omega_{eq} - \gamma \omega_i \sin^2 \alpha_{eq}}{\sin \alpha_{eq} \cos \alpha_{eq} (\gamma^2 - 1)} \Delta_{scat} I_i(\gamma, \alpha_{eq}), & \xi_i \in [\Pi_i(\gamma, \alpha_{eq}), 1] \\ \Delta_i \alpha_{eq} (\Delta_{trap} I_i, \gamma, \alpha_{eq}), & \xi_i \in [0, \Pi_i(\gamma, \alpha_{eq})] \end{cases}
 \end{aligned} \tag{3.9}$$

385

where ξ_i is a random variable uniformly distributed in $[0, 1]$. If there are two resonances (one with the first wave and another one with the second wave) during one electron bounce period τ_b , then over this period the electron energy/pitch-angle change should be

386

$$\begin{pmatrix} \bar{\gamma} \\ \bar{\alpha}_{eq} \end{pmatrix} = \begin{pmatrix} G_{\gamma 1}(G_{\gamma 0}(\gamma, \alpha_{eq}), G_{\alpha 0}(\gamma, \alpha_{eq})) \\ G_{\alpha 1}(G_{\gamma 0}(\gamma, \alpha_{eq}), G_{\alpha 0}(\gamma, \alpha_{eq})) \end{pmatrix} \tag{3.10}$$

388

Figure 8 shows ten main characteristics of map (3.10) in the energy/pitch-angle space: amplitudes of scattering $\Delta_{scat,i}\gamma$, $\Delta_{scat,i}\alpha_{eq}$, amplitudes of trapping $\Delta_{trap,i}\gamma$, $\Delta_{trap,i}\alpha_{eq}$, and trapping probabilities Π_i for two field-aligned whistler-mode waves. To derive these characteristics for given energy and pitch-angle, we (1) calculate γ , α_{eq} and resonance location s_R given by equation $I_i = I_{iR}$; (2) determine coefficients of Hamiltonian F_i , S , \dot{S} , and trapping probability Π at s_R ; (3) determine $\Delta_{scat} I_i = -S/2\pi$, position of escape from the resonance s_R^* (if $\dot{S}(s_R) > 0$), and $\Delta_{trap} I_i = I_{iR}(s_R^*) - I_{iR}(s_R)$; (4) recalculate $\Delta_{scat} I_i$, $\Delta_{trap} I_i$ into energy and pitch-angle changes. Numerical verification of this technique of $\Delta_{scat,i}\gamma$, $\Delta_{trap,i}\gamma$, Π_i with test particle trajectories can be found in Vainchtein *et al.* (2018); Artemyev *et al.* (2020b).

398

Substituting characteristics from Figure 8 into map (3.10), we evaluate dynamics of resonant electrons. Figure 9 shows a sample trajectory: energy and pitch-angle are plotted versus the number of iterations k and versus time $t = \sum_k \tau_{b,k}(\gamma, \alpha_{eq})$. The trajectory obtained with the mapping technique contains all elements that can be found in the numerically integrated trajectory (compare with Fig. 2): energy decrease due to phase

402

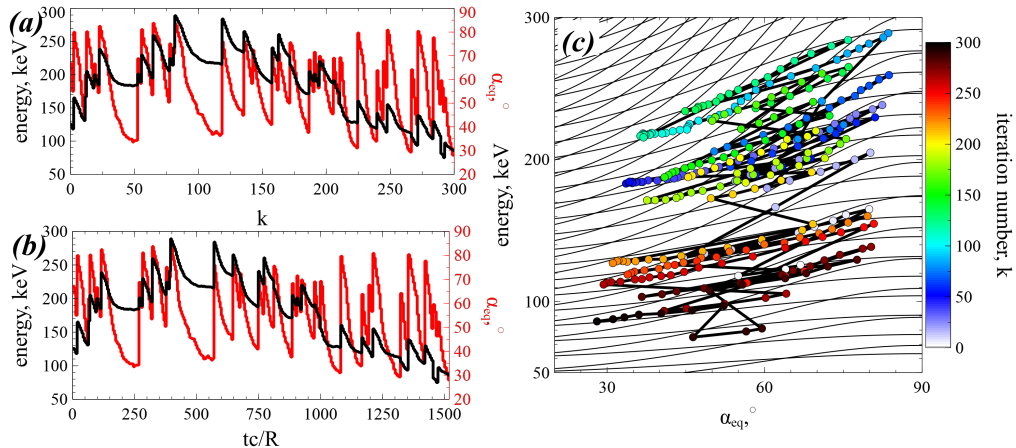


FIGURE 9. A sample trajectory obtained using map (3.10): energy and pitch-angle versus number of map iterations (a), energy and pitch-angle versus time (b), particle trajectory in the energy/pitch-angle space (c).

403 bunching and rare jumps due to phase trapping. Note that the bounce period is given
 404 by $\tau_b = 4 \int_0^{s_{\max}} ds/p$ with $p = m_e c^2 \sqrt{1 - \gamma - 2I_x \Omega_{ce}(s)}$ and $2I_x \Omega_{ce}(s_{\max}) = 1 - \gamma$.
 405 Any direct comparison of trajectories obtained via numerical integration and mapping
 406 technique is not possible due to significant randomization of resonant electron motion,
 407 i.e. trajectories in energy/pitch-angle plane for two test electrons can differ significantly
 408 even with small difference of initial electron phases (e.g., Shklyar 1981; Le Queau & Roux
 409 1987; Albert 2001). Thus, the verification of map (3.10) is mainly based on verification of
 410 Eqs. (3.5,3.7) (see Artemyev *et al.* 2015, 2016b; Vainchtein *et al.* 2018) and on verification
 411 of 1D analogs of this map (see Artemyev *et al.* 2020b).

412 Using map (3.10), we can simulate the evolution of the electron distribution function
 413 as an ensemble of test trajectories. We start with the test simulation of electron spread
 414 in the energy/pitch-angle space. Four populations of electrons with small ranges of
 415 initial energy and pitch-angles are traced for 500 interactions and their positions in
 416 energy/pitch-angle space are shown at six different times, see Fig. 10. White color
 417 shows the area of resonant wave-particle interaction (see Appendix B for a definition
 418 of this area and for technical details of map (3.10) application). Electrons of different
 419 initial populations quickly (already after $tc/R \sim 50$, i.e., ~ 15 resonant interactions)
 420 spread within a wide pitch-angle range, but are somehow separated in energy. After
 421 $tc/R \sim 300$ (~ 80 resonant interactions) the populations fill large areas in energy/pitch-
 422 angle space and start overlapping. After $tc/R \sim 1000$ (~ 250 resonant interactions) the
 423 entire energy/pitch-angle space is covered, and electrons from low energy populations
 424 (black and blue) reach high energies (~ 1 MeV), whereas electrons from high-energy
 425 populations (red and magenta) decelerate with energy losses of several hundred keVs.
 426 Such fast phase mixing should result in spreading and smoothing of the electron phase
 427 space density.

428 To examine the evolution of the electron phase space density, we start with a power
 429 law distribution $f_0(\gamma, \alpha) = C \cdot \sin \alpha_{eq} \cdot (\gamma - 1)^{-3}$ typical in the radiation belts, and fit
 430 this distribution by $2 \cdot 10^7$ trajectories. There are 180×400 pitch-angle/energy values,
 431 and ~ 22600 within the resonant area; for each value within the resonant area, we run
 432 1000 trajectories. Each trajectory is traced for 300 interactions with the map (3.10),
 433 and corresponding $\alpha_{eq}(k)$, $\gamma(k)$ profiles transferred to time series. Then, we recalculate

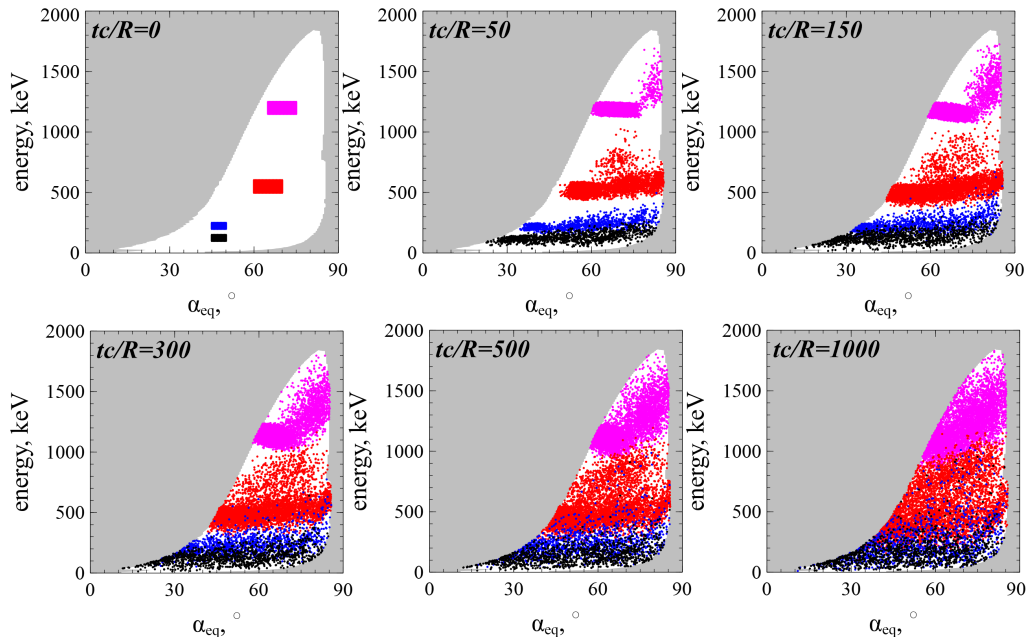


FIGURE 10. Evolution of four electron populations modeled with map (3.10). Six moments of time are shown. White color shows the area of wave-particle nonlinear resonant interaction, see Appendix B.

434 the distribution from f_0 using phase space density conservation along the trajectories.
 435 Figure 11 shows three snapshots of the distribution $f(\alpha, \gamma)$ at different times (inserted
 436 panels show the low energy sub-interval). The rapid evolution of the distribution function
 437 results in phase space density flattening within the resonant region: there is an increase
 438 of high-energy/small pitch-angle phase space density and a decrease of low energy/large
 439 pitch-angle phase space density. During the simulation time, one electron can be trapped
 440 several times, i.e., most of particles circulate in the energy/pitch-angle space, because
 441 trappings bring them to the high energy region from which they then drift by bunching.
 442 Such a circulation also comprises successive trappings by two waves that bring electrons
 443 to the very high-energy region, whereas long periods of phase bunching without trappings
 444 can transport very energetic electrons to quite low energies. The last two phenomena are
 445 less frequent, and mixing of ~ 1 MeV electrons with < 100 keV electrons is slower than
 446 mixing within energy localized domains.

447 The general trend of the resonant electron transport in the energy/pitch-angle space
 448 is the reduction of phase space density gradients. In the presence of a single wave, such a
 449 gradient smoothing occurs along the resonant curves, $\gamma - \omega_0 I_0 = \text{const}$ (Artemyev *et al.*
 450 2020b). In systems with two waves, the intersection of resonant curves $\gamma - \omega_0 I_0 = \text{const}$
 451 and $\gamma - \omega_1 I_1 = \text{const}$ results in 2D gradient smoothing, i.e., we can expect a reduction of
 452 gradients in energy space after integration over pitch-angle. Figure 12 shows such electron
 453 acceleration: increase of high-energy population and decrease of low energy population
 454 that result in gradient smoothing. This is the typical evolution of the electron distribution
 455 due to resonant interaction with whistler-mode waves (see similar results for nonlinear
 456 (Vainchtein *et al.* 2018) and quasi-linear (Thorne *et al.* 2013; Li *et al.* 2014) simulations).

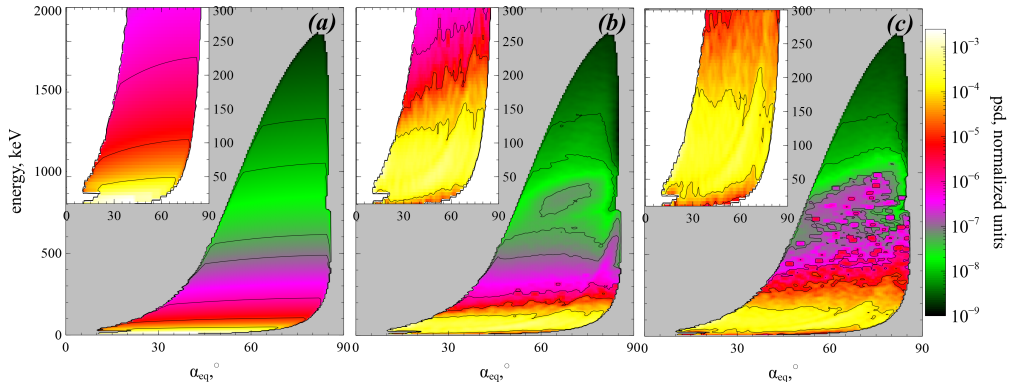


FIGURE 11. Evolution of electron distribution modeled with map (3.10). Three moments of time are shown: $tc/R = 0$ (a), $tc/R = 300$ (b), $tc/R = 1000$ (c). The initial distribution $f_0(\gamma, \alpha) = C \cdot \sin \alpha_{eq} \cdot (\gamma - 1)^{-3}$ in panel (a).

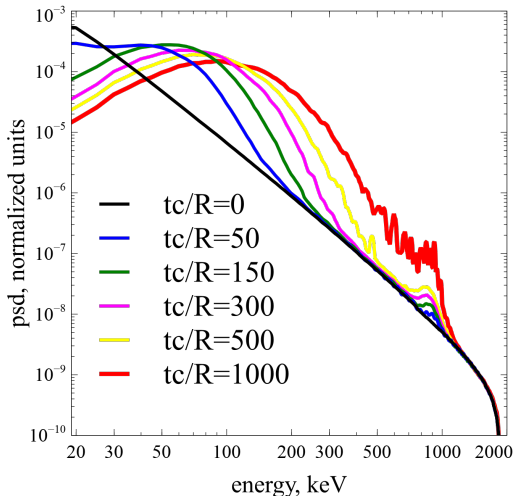


FIGURE 12. Pitch-angle integrated electron distribution, $\int_0^\pi \sin \alpha_{eq} \cdot psd(E, \alpha_{eq}) d\alpha_{eq}$, from Fig. 11.

4. Discussion and conclusions

457
 458 The proposed approach allows to investigate the long-term evolution of the electron
 459 distribution function in a system with nonlinear wave-particle interaction. This approach
 460 is based on the mapping technique that significantly simplifies electron trajectory integra-
 461 tion by excluding from the consideration the main, adiabatic part of electron orbits and
 462 by focusing only on small intervals of resonant electron phase bunching and trapping. This
 463 approach is somewhat analogous to the Green function method proposed by (Furuya *et al.*
 464 2008; Omura *et al.* 2015) and to the nonlinear kinetic equation proposed by (Artemyev
 465 *et al.* 2016b; Vainchtein *et al.* 2018). However, contrary to these other methods, the
 466 mapping does not require a very fine discretization of energy/pitch-angle space and it
 467 can easily be generalized to multi-wave systems. Resonances with different waves are
 468 very important for the destruction of the symmetry typical for the single wave system,
 469 where conservation of $(\gamma - \omega I)$ results in a reduced mixing in energy/pitch-angle space.
 470 Already, two waves with different characteristics are sufficient to produce a total mixing
 471 in energy/pitch-angle space (see Fig. 10) and a smoothing (reduction) of electron phase

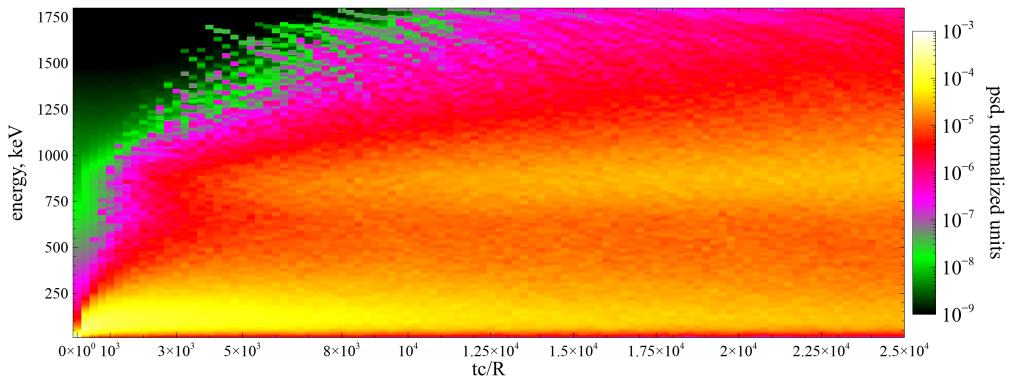


FIGURE 13. Evolution of pitch-angle integrated electron distribution, $\int_0^\pi \sin \alpha_{eq} \cdot psd(E, \alpha_{eq}) d\alpha_{eq}$ in a long-term simulation.

472 space density gradients (see Figure 12). The similar effect of fast mixing due to two
 473 independent resonances has been found in various dynamical systems with quite general
 474 properties (e.g. Gelfreich *et al.* 2011; Itin & Neishtadt 2012).

475 Moreover, note that our simulations shown in Figures 9-12 are quite localized in time,
 476 since $R/c \sim 1000$ is about 100 s in the outer radiation belt ($L \sim 5$), and that this time
 477 period is much smaller than the characteristic time of evolution of any process typically
 478 modelled by quasi-linear theory (Thorne *et al.* 2013; Drozdov *et al.* 2015; Albert *et al.*
 479 2016; Ma *et al.* 2016, 2018). Therefore, we extend the simulation interval to $tc/R =$
 480 $2.5 \cdot 10^4$ (~ 40 min) to show that this time scale is already sufficiently long to almost
 481 fully smooth gradients within < 1 MeV, see Fig. 13. Generally, however, 40 minutes is a
 482 too long interval to keep whistler-mode wave activity at the same high level (although
 483 such long-living regions of intense waves are sometimes observed, see Cully *et al.* (2008);
 484 Agapitov *et al.* (2015b); Cattell *et al.* (2015)).

485 Figure 8 shows energy/pitch-angle domains of nonlinear wave-particle interaction, and
 486 these domains are used for the simulation of the electron distribution function evolution
 487 (see Figures 10-13 and Appendix C). For simplicity, we assume that the boundary of these
 488 domains is impenetrable. However, additionally to nonlinear wave-particle interactions
 489 (phase bunching and phase trapping), there is also in reality some electron diffusion. This
 490 diffusion is finite everywhere in the energy/pitch-angle plane where there is an electron
 491 resonance with the whistler-mode wave. Thus, this diffusion would transport electrons
 492 across the boundary of the domains of nonlinear wave-particle interaction. The direction
 493 of this transport depends on the phase space density gradients. At low energies, the
 494 nonlinear wave-particle interaction results in phase space density decrease (see Fig. 13),
 495 and thus pitch-angle diffusion will bring new small-energy particles into these domains.
 496 At high energies, the nonlinear wave-particle interaction results in phase space density
 497 increase (see Fig. 13), and thus both energy and pitch-angle diffusion will try to spread
 498 this phase space density maximum. Such diffusion can be included into the map (3.10)
 499 as random energy and pitch-angle jumps with zero mean values and amplitudes given
 500 by the quasi-linear model (e.g., Albert 2010). However, the diffusion is generally much
 501 weaker than nonlinear phase bunching and trapping, and the diffusion-driven evolution
 502 of the phase space density should mostly appear after nonlinear wave-particle interaction
 503 has already partly smoothed the initial phase space density gradients (Artemyev *et al.*
 504 2019a).

505 The map (3.10) has been constructed for electron interaction with monochromatic

waves (see Eq. (2.1)), whereas spacecraft observations in the Earths radiation belts often report about more complex wave field distributions, e.g., significant wave amplitude modulation (Tao *et al.* 2013; Santolík *et al.* 2014; Zhang *et al.* 2018, 2019), accompanied by fast, strong, and random variations of wave frequency and phase (Zhang *et al.* 2020*b,a*), often resulting in the formation of almost independent short wave packets or sub-packets (Mourenas *et al.* 2018; Zhang *et al.* 2020*a*). Such a chaotization of wave fields is likely partly driven by currents of resonant electrons (Nunn *et al.* 2009; Demekhov 2011; Katoh & Omura 2011, 2016; Tao *et al.* 2017; Tao *et al.* 2020) and sideband instability (Nunn 1986), as well as by the simultaneous excitation of at least two different waves with a significant frequency difference (Katoh & Omura 2013; Crabtree *et al.* 2017; Zhang *et al.* 2020*b*). Since phase bunching is a local process, wave modulation cannot affect the theoretical model of energy and pitch-angle jumps due to bunching, but the inclusion of such a modulation into the 2-wave model map would require some probabilistic distribution of wave amplitudes within short wave packets. The situation is more complicated for phase trapping, which is nonlocal and depends on wave packet size and amplitude modulation within the packets (Mourenas *et al.* 2018). Test particle simulations demonstrate that wave modulation alone makes phase trapping less efficient for electron acceleration, but increases the probability of phase trapping (Kubota & Omura 2018; Gan *et al.* 2020*a*; Zhang *et al.* 2020*a*). Thus, an important further development of the mapping technique for nonlinear wave-particle interaction would require modifications of the phase trapping model.

Another important constraint for trapping efficiency is related to the resonance overlapping in the multi-wave system. We restrict our consideration to the case of well separated resonances; however, spacecraft observations often report the presence of quite broadband whistler-mode emission where resonances of two neighboring waves can overlap (see discussion in, e.g., Summers *et al.* (2014); Tong *et al.* (2019)). Such resonance overlapping should enhance the electron diffusion, but destroy the phase trapping (e.g., Karimabadi *et al.* (1990); Artemyev *et al.* (2010); Shklyar & Zimbardo (2014)). In the absence of trapping resonant systems can be described by the simple Fokker-Plank equation (Sagdeev *et al.* 1988; Lichtenberg & Lieberman 1983), i.e. the mapping technique described within this study can be reduced to a standard map. The most natural partial overlapping would result in a quite complex situation where the assumption of the resonant phase randomization (the basic assumption of the described map) could be violated. Such systems would be described by fractional Fokker-Plank equations (e.g., Zelenyi & Milovanov (2004); Zaslavsky (2005); Isliker *et al.* (2017)), and this is a poorly investigated topic in application to the physics of resonant wave-particle interaction.

To conclude, we have demonstrated the usefulness of the mapping technique for Hamiltonian systems describing nonlinear resonant interaction of charged particles and intense electromagnetic waves. We have shown that in systems with two (and more) waves, the resonant interaction destroys the symmetries of the single wave resonance and drives a rapid smoothing of particle phase space density gradients. The proposed approach appears very promising for the investigation of relativistic electron interaction with various intense whistler-mode waves and EMIC waves in the Earths radiation belts (Katoh & Omura 2013; Mourenas *et al.* 2016*a,b*; Ma *et al.* 2017; He *et al.* 2020; Yu *et al.* 2020; Zhang *et al.* 2020*b*) or in the solar wind (Wilson *et al.* 2007, 2013; Krafft *et al.* 2013; Krafft & Volokitin 2016; Tong *et al.* 2019; Roberg-Clark *et al.* 2019). It could be useful also for studying electron acceleration by simultaneous laser-driven plasma waves (Modena *et al.* 1995; Tikhonchuk 2019), and electron precipitation driven by VLF waves generated by electron beams or antennas in space (Carlsten *et al.* 2019; Borovsky *et al.* 2020).

Acknowledgements

The work of A.V.A., A.I.N., and A.A.V. was supported by Russian Scientific Foundation (project no. 19-12-00313). The work of A.V.A and X.J.Z. was also supported in part by NSF grant 2021749 and NASA grant 80NSSC20K1270. The work of X.J.Z. and D.L.V. was supported by NASA grants 80NSSC20K1578 and 80NSSC19K0266. The work of A.I.N. was supported in part by the Leverhulme Trust grant RPG-2018-143.

Appendix A

Equation (3.6) describes energy decrease due to phase bunching, and natural limitation of this equation is that $\gamma + \Delta\gamma$ should be larger than one; or, alternatively, $I_x + (m_e c^2/\omega)\Delta\gamma$ should be larger than zero. This effect of drift asymmetry, i.e. absence of electron drift to negative I_x , has been noticed by Lundin & Shkliar (1977) who showed that for very small I_x the phase bunching change the drift direction. This effect is called anomalous phase bunching (Kitahara & Katoh 2019; Grach & Demekhov 2020; Gan *et al.* 2020a) and basically consists in positive I_x (and γ) changes due to bunching at very small I_x . Theoretically, the parametrical boundary of anomalous bunching in energy/pitch-angle space is determined by $I_x < I_x^*$ with I_x^* scaling as $(B_w/B_0)^{2/3}$. Let us derive this scaling, but leave the more detailed consideration of small I_x phase bunching to further consideration. We start with Eq. (2.5) written for a single wave

$$H_I = -\omega I + m_e c^2 \gamma + \sqrt{\frac{2I\Omega_{ce}}{m_e c^2}} \frac{e B_w}{\gamma k} \sin \varphi, \quad \gamma = \sqrt{1 + \frac{(P + kI)^2}{m_e^2 c^2} + \frac{2I\Omega_{ce}}{m_e c^2}} \quad (4.1)$$

Hamiltonian equations for I and φ take the form:

$$\dot{I} = -\sqrt{\frac{2I\Omega_{ce}}{m_e c^2}} \frac{e B_w}{k\gamma} \sin \varphi, \quad \dot{\varphi} = \frac{k^2}{\gamma m_e} (I - I_R) + \sqrt{\frac{\Omega_{ce}}{2I m_e c^2}} \frac{e B_w}{k\gamma} \sin \varphi \quad (4.2)$$

where $I_R = (\gamma\omega m_e - P)/k$ is the solution of $\partial H/\partial I = 0$ equation for $B_w = 0$. Equation (4.2) describes fast phase rotation (with frequency $k^2(I - I_R)/\gamma m_e$) and I, φ evolution driven by much weaker wave force $\sim B_w/B_0$. Until I (and I_R) are sufficiently large to keep this time separation, we can apply the theory of phase bunching resulting in Eq. (3.6). However, let us consider small I, I_R values. We introduce a small parameter $\varepsilon = B_w/B_0$ and normalized $(\tilde{I}, \tilde{I}_R) = (I, I_R)/\varepsilon^\beta$:

$$\frac{d\tilde{I}}{dt} = -\sqrt{\frac{2\tilde{I}\Omega_{ce}}{m_e c^2}} \frac{e B_0}{k\gamma} \varepsilon^{1-\beta/2} \sin \varphi, \quad \frac{d\varphi}{dt} = \frac{k^2 \varepsilon^\beta}{\gamma m_e} (\tilde{I} - \tilde{I}_R) + \sqrt{\frac{\Omega_{ce}}{2\tilde{I} m_e c^2}} \frac{e B_0}{k\gamma} \varepsilon^{1-\beta/2} \sin \varphi \quad (4.3)$$

Introducing slow time $\tau = t\varepsilon^{1-\beta/2}$, we obtain

$$\frac{d\tilde{I}}{d\tau} = -\sqrt{\frac{2\tilde{I}\Omega_{ce}}{m_e c^2}} \frac{e B_0}{k\gamma} \sin \varphi, \quad \frac{d\varphi}{d\tau} = \frac{k^2}{\gamma m_e} (\tilde{I} - \tilde{I}_R) \varepsilon^{3\beta/2-1} + \sqrt{\frac{\Omega_{ce}}{2\tilde{I} m_e c^2}} \frac{e B_0}{k\gamma} \sin \varphi \quad (4.4)$$

Thus, for $\beta = 2/3$ Eqs. (4.4) lose the small parameter, and \tilde{I}, φ would change with the same rate. Then the applicability of equations of the phase bunching theory breaks, and a new model for ΔI (or $\Delta\gamma, \Delta I_x$) is required. $\beta = 2/3$ gives the threshold value for $I_x \sim I \sim (B_w/B_0)^\beta$.

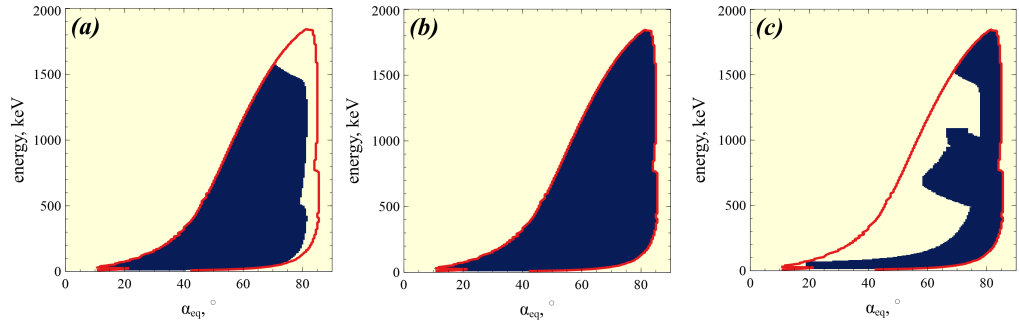


FIGURE 14. Domains in energy/pitch-angle space with: positive probability of trapping (a), a finite phase bunching energy/pitch-angle change (b), positions of release from the trapping (c). Red curve shows boundary of (b) domain.

Appendix B

Figure 8 shows that there are certain domains in the energy/pitch-angle space where electrons resonate with whistler wave nonlinearly. Thus, simulation of resonant electron dynamics should be within these domains. Figure 14(b) shows the largest domain that cover all energies and pitch-angles where electrons experience phase bunching. The phase bunching results in energy/pitch-angle change and electron drifts within the domain. Important property of the domain boundary is that $\Delta_{scat}\gamma$ tends there to zero as $\sim (I - I_{boundary})^{4/3}$ where I and $I_{boundary}$ are values of moment and its boundary value (Artemyev *et al.* 2019a), i.e. $\Delta\gamma$ drops to zero at the domain boundary and no particles should leave this domain (in absence of diffusion that is characterized by a finite diffusion coefficient within the entire energy/pitch-angle space). As $\Delta_{scat}\gamma$ has been derived numerically, there are possible fluctuations making $\Delta_{scat}\gamma$ finite at the boundary. Thus, distribution $\Delta\gamma(E, \alpha_{eq})$ should be corrected to set $\Delta_{scat}\gamma = 0$ at the domain boundary. Moreover, if during the simulation resonant electrons escape from the domain of phase bunching (e.g., because of numerical effects), these electrons should be returned into the domain (e.g., reflecting them back from the boundary on the same $\Delta_{scat}\gamma$). Note that this procedure is required only in the absence of particle diffusion. †

The domain of a finite trapping probability is smaller than the bunching domain (see Fig. 14(a)). Again, the probability of trapping tends to zero at the phase bunching domain boundary as $\Pi \sim (I - I_{boundary})^{1/3}$ (Artemyev *et al.* 2019a), and Π should be set equal to zero on this boundary even if numerical fluctuations of Π evaluation give some finite value. Of course, there are no regions with $\Pi > 0$ outside the phase bunching domain.

Release of trapped electrons from the resonance also should be within the phase bunching domain (see Fig. 14(c)). Numerical errors put some release locations outside this domain; the trapping variation $\Delta_{trap}\gamma$ should be corrected to move the release locations within the domain. This guarantees that for each energy/pitch-angle within the phase bunching domain we would have incoming and outgoing phase space flows.

REFERENCES

- AGAPITOV, O. V., ARTEMYEV, A., KRASNOSELSKIKH, V., KHOTYAINTSEV, Y. V., MOURENAS, D., BREUILLARD, H., BALIKHIN, M. & ROLLAND, G. 2013 Statistics of whistler mode

† The system has 3 degrees of freedom. Thus, generally there are deviations from adiabatic trajectories even for non-resonant motions due to the Arnold diffusion (Arnold *et al.* (2006)). However, this diffusion is exponentially slow and can be neglected here.

- 615 waves in the outer radiation belt: Cluster STAFF-SA measurements. *J. Geophys. Res.*
 616 **118**, 3407–3420.
- 617 AGAPITOV, O. V., ARTEMYEV, A., MOURENAS, D., KRASNOSELSKIKH, V., BONNELL, J., LE
 618 CONTEL, O., CULLY, C. M. & ANGELOPOULOS, V. 2014 The quasi-electrostatic mode of
 619 chorus waves and electron nonlinear acceleration. *J. Geophys. Res.* **119**, 1606–1626.
- 620 AGAPITOV, O. V., ARTEMYEV, A. V., MOURENAS, D., MOZER, F. S. & KRASNOSELSKIKH,
 621 V. 2015a Empirical model of lower band chorus wave distribution in the outer radiation
 622 belt. *J. Geophys. Res.* **120**, 10.
- 623 AGAPITOV, O. V., ARTEMYEV, A. V., MOURENAS, D., MOZER, F. S. & KRASNOSELSKIKH,
 624 V. 2015b Nonlinear local parallel acceleration of electrons through Landau trapping by
 625 oblique whistler mode waves in the outer radiation belt. *Geophys. Res. Lett.* **42**, 10.
- 626 ALBERT, J. M. 1993 Cyclotron resonance in an inhomogeneous magnetic field. *Physics of Fluids*
 627 *B* **5**, 2744–2750.
- 628 ALBERT, J. M. 2001 Comparison of pitch angle diffusion by turbulent and monochromatic
 629 whistler waves. *J. Geophys. Res.* **106**, 8477–8482.
- 630 ALBERT, J. M. 2010 Diffusion by one wave and by many waves. *J. Geophys. Res.* **115**, 0.
- 631 ALBERT, J. M., STARKS, M. J., HORNE, R. B., MEREDITH, N. P. & GLAUERT, S. A.
 632 2016 Quasi-linear simulations of inner radiation belt electron pitch angle and energy
 633 distributions. *Geophys. Res. Lett.* **43**, 2381–2388.
- 634 ALBERT, J. M., TAO, X. & BORTNIK, J. 2013 Aspects of Nonlinear Wave-Particle Interactions.
 635 In *Dynamics of the Earth's Radiation Belts and Inner Magnetosphere* (ed. D. Summers,
 636 I. U. Mann, D. N. Baker & M. Schulz).
- 637 ALLANSON, O., WATT, C. E. J., RATCLIFFE, H., ALLISON, H. J., MEREDITH, N. P., BENTLEY,
 638 S. N., ROSS, J. P. J. & GLAUERT, S. A. 2020 Particle-in-Cell Experiments Examine
 639 Electron Diffusion by Whistler-Mode Waves: 2. Quasi-Linear and Nonlinear Dynamics.
 640 *Journal of Geophysical Research (Space Physics)* **125** (7), e27949.
- 641 ANDRONOV, A. A. & TRAKHTENGERTS, V. Y. 1964 Kinetic instability of the Earth's outer
 642 radiation belt. *Geomagnetism and Aeronomy* **4**, 233–242.
- 643 ARNOLD, V. I., KOZLOV, V. V. & NEISHTADT, A. I. 2006 *Mathematical Aspects of Classical*
 644 *and Celestial Mechanics*, 3rd edn. New York: Springer-Verlag.
- 645 ARTEMYEV, A. V., AGAPITOV, O., MOURENAS, D., KRASNOSELSKIKH, V., SHASTUN, V. &
 646 MOZER, F. 2016a Oblique Whistler-Mode Waves in the Earth's Inner Magnetosphere:
 647 Energy Distribution, Origins, and Role in Radiation Belt Dynamics. *Space Sci. Rev.*
 648 **200** (1-4), 261–355.
- 649 ARTEMYEV, A. V., NEISHTADT, A. I., VAINCHTEIN, D. L., VASILIEV, A. A., VASKO, I. Y. &
 650 ZELENYI, L. M. 2018a Trapping (capture) into resonance and scattering on resonance:
 651 Summary of results for space plasma systems. *Communications in Nonlinear Science and*
 652 *Numerical Simulations* **65**, 111–160.
- 653 ARTEMYEV, A. V., NEISHTADT, A. I. & VASILIEV, A. A. 2019a Kinetic equation for
 654 nonlinear wave-particle interaction: Solution properties and asymptotic dynamics. *Physica*
 655 *D Nonlinear Phenomena* **393**, 1–8, arXiv: 1809.03743.
- 656 ARTEMYEV, A. V., NEISHTADT, A. I. & VASILIEV, A. A. 2020a A Map for Systems with
 657 Resonant Trappings and Scatterings. *Regular and Chaotic Dynamics* **25** (1), 2–10.
- 658 ARTEMYEV, A. V., NEISHTADT, A. I. & VASILIEV, A. A. 2020b Mapping for nonlinear
 659 electron interaction with whistler-mode waves. *Physics of Plasmas* **27** (4), 042902, arXiv:
 660 1911.11459.
- 661 ARTEMYEV, A. V., NEISHTADT, A. I., VASILIEV, A. A. & MOURENAS, D. 2016b Kinetic
 662 equation for nonlinear resonant wave-particle interaction. *Physics of Plasmas* **23** (9),
 663 090701.
- 664 ARTEMYEV, A. V., NEISHTADT, A. I., VASILIEV, A. A. & MOURENAS, D. 2017 Probabilistic
 665 approach to nonlinear wave-particle resonant interaction. *Phys. Rev. E* **95** (2), 023204.
- 666 ARTEMYEV, A. V., NEISHTADT, A. I., VASILIEV, A. A. & MOURENAS, D. 2018b Long-term
 667 evolution of electron distribution function due to nonlinear resonant interaction with
 668 whistler mode waves. *Journal of Plasma Physics* **84**, 905840206.
- 669 ARTEMYEV, A. V., NEISHTADT, A. I., ZELENYI, L. M. & VAINCHTEIN, D. L. 2010 Adiabatic
 670 description of capture into resonance and surfatron acceleration of charged particles by
 671 electromagnetic waves. *Chaos* **20** (4), 043128.

- 672 ARTEMYEV, A. V., VASILIEV, A. A., MOURENAS, D., AGAPITOV, O. & KRASNOSELSKIKH,
673 V. 2013 Nonlinear electron acceleration by oblique whistler waves: Landau resonance vs.
674 cyclotron resonance. *Physics of Plasmas* **20**, 122901.
- 675 ARTEMYEV, A. V., VASILIEV, A. A., MOURENAS, D., AGAPITOV, O., KRASNOSELSKIKH, V.,
676 BOSCHER, D. & ROLLAND, G. 2014a Fast transport of resonant electrons in phase space
677 due to nonlinear trapping by whistler waves. *Geophys. Res. Lett.* **41**, 5727–5733.
- 678 ARTEMYEV, A. V., VASILIEV, A. A., MOURENAS, D., AGAPITOV, O. V. & KRASNOSELSKIKH,
679 V. V. 2014b Electron scattering and nonlinear trapping by oblique whistler waves: The
680 critical wave intensity for nonlinear effects. *Physics of Plasmas* **21** (10), 102903.
- 681 ARTEMYEV, A. V., VASILIEV, A. A., MOURENAS, D., NEISHTADT, A. I., AGAPITOV, O. V.
682 & KRASNOSELSKIKH, V. 2015 Probability of relativistic electron trapping by parallel
683 and oblique whistler-mode waves in Earth’s radiation belts. *Physics of Plasmas* **22** (11),
684 112903.
- 685 ARTEMYEV, A. V., VASILIEV, A. A. & NEISHTADT, A. I. 2019b Charged particle nonlinear
686 resonance with localized electrostatic wave-packets. *Communications in Nonlinear Science
687 and Numerical Simulations* **72**, 392–406.
- 688 BALIKHIN, M. A., DE WIT, T. D., ALLEYNE, H. S. C. K., WOOLLISCROFT, L. J. C., WALKER,
689 S. N., KRASNOSELSKIKH, V., MIER-JEDRZEJEOWICZ, W. A. C. & BAUMJOHANN, W.
690 1997 Experimental determination of the dispersion of waves observed upstream of a quasi-
691 perpendicular shock. *Geophys. Res. Lett.* **24**, 787–790.
- 692 BELL, T. F. 1984 The nonlinear gyroresonance interaction between energetic electrons and
693 coherent VLF waves propagating at an arbitrary angle with respect to the earth’s magnetic
694 field. *J. Geophys. Res.* **89**, 905–918.
- 695 BENKADDA, S., SEN, A. & SHKLYAR, D. R. 1996 Chaotic dynamics of charged particles in the
696 field of two monochromatic waves in a magnetized plasma. *Chaos* **6** (3), 451–460.
- 697 BOROVSKY, J. E., DELZANNO, G. L., DORS, E. E., THOMSEN, M. F., SANCHEZ, E. R.,
698 HENDERSON, M. G., MARSHALL, R. A., GILCHRIST, B. E., MIARS, G., CARLSTEN, B. E.,
699 STORMS, S. A., HOLLOWAY, M. A. & NGUYEN, D. 2020 Solving the auroral-arc-generator
700 question by using an electron beam to unambiguously connect critical magnetospheric
701 measurements to auroral images. *Journal of Atmospheric and Solar-Terrestrial Physics*
702 **206**, 105310.
- 703 CAMPOREALE, E. & ZIMBARDO, G. 2015 Wave-particle interactions with parallel whistler waves:
704 Nonlinear and time-dependent effects revealed by particle-in-cell simulations. *Physics of
705 Plasmas* **22** (9), 092104, arXiv: 1412.3229.
- 706 CARLSTEN, B. E., COLESTOCK, P. L., CUNNINGHAM, G. S., DELZANNO, G. L., DORS, E. E.,
707 HOLLOWAY, M. A., JEFFERY, C. A., LEWELLEN, J. W., MARKSTEINER, Q. R., NGUYEN,
708 D. C., REEVES, G. D. & SHIPMAN, K. A. 2019 Radiation-Belt Remediation Using Space-
709 Based Antennas and Electron Beams. *IEEE Transactions on Plasma Science* **47** (5),
710 2045–2063.
- 711 CATTELL, C., WYGANT, J. R., GOETZ, K., KERSTEN, K., KELLOGG, P. J., VON ROSENVINGE,
712 T., BALE, S. D., ROTH, I., TEMERIN, M., HUDSON, M. K., MEWALDT, R. A.,
713 WIEDENBECK, M., MAKSIMOVIC, M., ERGUN, R., ACUNA, M. & RUSSELL, C. T.
714 2008 Discovery of very large amplitude whistler-mode waves in Earth’s radiation belts.
715 *Geophys. Res. Lett.* **35**, 1105.
- 716 CATTELL, C. A., BRENNEMAN, A. W., THALLER, S. A., WYGANT, J. R., KLETZING, C. A. &
717 KURTH, W. S. 2015 Van Allen Probes observations of unusually low frequency whistler
718 mode waves observed in association with moderate magnetic storms: Statistical study.
719 *Geophys. Res. Lett.* **42**, 7273–7281.
- 720 CHASTON, C. C., SALEM, C., BONNELL, J. W., CARLSON, C. W., ERGUN, R. E., STRANGWAY,
721 R. J. & MCFADDEN, J. P. 2008 The Turbulent Alfvénic Aurora. *Physical Review Letters*
722 **100** (17), 175003.
- 723 CHEN, L., BRENNEMAN, A. W., XIA, Z. & ZHANG, X.-J. 2020 Modeling of Bouncing Electron
724 Microbursts Induced by Ducted Chorus Waves. *Geophys. Res. Lett.* **47** (17), e89400.
- 725 CHEN, L., ZHU, H. & ZHANG, X. 2019 Wavenumber Analysis of EMIC Waves. *Geophys. Res.
726 Lett.* **46** (11), 5689–5697.
- 727 CHIRIKOV, B. V. 1979 A universal instability of many-dimensional oscillator systems. *Physics
728 Reports* **52**, 263–379.
- 729 CRABTREE, C., TEJERO, E., GANGULI, G., HOSPODARSKY, G. B. & KLETZING, C. A. 2017

- 730 Bayesian spectral analysis of chorus subelements from the Van Allen Probes. *Journal of*
731 *Geophysical Research (Space Physics)* **122** (6), 6088–6106.
- 732 CULLY, C. M., ANGELOPOULOS, V., AUSTER, U., BONNELL, J. & LE CONTEL, O. 2011
733 Observational evidence of the generation mechanism for rising-tone chorus. *Geophys.*
734 *Res. Lett.* **38**, 1106.
- 735 CULLY, C. M., BONNELL, J. W. & ERGUN, R. E. 2008 THEMIS observations of long-lived
736 regions of large-amplitude whistler waves in the inner magnetosphere. *Geophys. Res.*
737 *Lett.* **35**, 17.
- 738 DEMEKHOV, A. G. 2011 Generation of VLF emissions with the increasing and decreasing
739 frequency in the magnetospheric cyclotron maser in the backward wave oscillator regime.
740 *Radiophysics and Quantum Electronics* **53**, 609–622.
- 741 DEMEKHOV, A. G., TRAKHTENGERTS, V. Y., RYCROFT, M. & NUNN, D. 2009 Efficiency of
742 electron acceleration in the Earth’s magnetosphere by whistler mode waves. *Geomagnetism*
743 *and Aeronomy* **49**, 24–29.
- 744 DEMEKHOV, A. G., TRAKHTENGERTS, V. Y., RYCROFT, M. J. & NUNN, D. 2006 Electron
745 acceleration in the magnetosphere by whistler-mode waves of varying frequency.
746 *Geomagnetism and Aeronomy* **46**, 711–716.
- 747 DROZDOV, A. Y., SHPRITS, Y. Y., ORLOVA, K. G., KELLERMAN, A. C., SUBBOTIN, D. A.,
748 BAKER, D. N., SPENCE, H. E. & REEVES, G. D. 2015 Energetic, relativistic, and
749 ultrarelativistic electrons: Comparison of long-term VERB code simulations with Van
750 Allen Probes measurements. *J. Geophys. Res.* **120**, 3574–3587.
- 751 DRUMMOND, W. E. & PINES, D. 1962 Nonlinear stability of plasma oscillations. *Nuclear Fusion*
752 *Suppl.* **3**, 1049–1058.
- 753 FOSTER, J. C., ERICKSON, P. J., BAKER, D. N., CLAUDEPIERRE, S. G., KLETZING, C. A.,
754 KURTH, W., REEVES, G. D., THALLER, S. A., SPENCE, H. E., SHPRITS, Y. Y. &
755 WYGANT, J. R. 2014 Prompt energization of relativistic and highly relativistic electrons
756 during a substorm interval: Van Allen Probes observations. *Geophys. Res. Lett.* **41**,
757 20–25.
- 758 FURUYA, N., OMURA, Y. & SUMMERS, D. 2008 Relativistic turning acceleration of radiation
759 belt electrons by whistler mode chorus. *J. Geophys. Res.* **113**, 4224.
- 760 GAN, L., LI, W., MA, Q., ALBERT, J. M., ARTEMYEV, A. V. & BORTNIK, J. 2020a Nonlinear
761 Interactions Between Radiation Belt Electrons and Chorus Waves: Dependence on Wave
762 Amplitude Modulation. *Geophys. Res. Lett.* **47** (4), e85987.
- 763 GAN, L., LI, W., MA, Q., ARTEMYEV, A. V. & ALBERT, J. M. 2020b Unraveling the
764 Formation Mechanism for the Bursts of Electron Butterfly Distributions: Test Particle
765 and Quasilinear Simulations. *Geophys. Res. Lett.* **47** (21), e90749.
- 766 GELFREICH, V., ROM-KEDAR, V., SHAH, K. & TURAEV, D. 2011 Robust Exponential
767 Acceleration in Time-Dependent Billiards. *Phys. Rev. Lett.* **106** (7), 074101.
- 768 GRACH, V. S. & DEMEKHOV, A. G. 2018 Resonance Interaction of Relativistic Electrons
769 with Ion-Cyclotron Waves. I. Specific Features of the Nonlinear Interaction Regimes.
770 *Radiophysics and Quantum Electronics* **60** (12), 942–959.
- 771 GRACH, V. S. & DEMEKHOV, A. G. 2020 Precipitation of Relativistic Electrons Under Resonant
772 Interaction With Electromagnetic Ion Cyclotron Wave Packets. *Journal of Geophysical*
773 *Research (Space Physics)* **125** (2), e27358.
- 774 HE, Z., YAN, Q., ZHANG, X., YU, J., MA, Y., CAO, Y. & CUI, J. 2020 Precipitation loss
775 of radiation belt electrons by two-band plasmaspheric hiss waves. *Journal of Geophysical*
776 *Research: Space Physics* p. e2020JA028157.
- 777 HIRAGA, R. & OMURA, Y. 2020 Acceleration mechanism of radiation belt electrons through
778 interaction with multi-subpacket chorus waves. *Earth, Planets, and Space* **72** (1), 21.
- 779 HSIEH, Y.-K., KUBOTA, Y. & OMURA, Y. 2020 Nonlinear evolution of radiation belt electron
780 fluxes interacting with oblique whistler mode chorus emissions. *Journal of Geophysical*
781 *Research: Space Physics* p. e2019JA027465, 2019JA027465
- 782 HSIEH, Y.-K. & OMURA, Y. 2017 Nonlinear dynamics of electrons interacting with oblique
783 whistler mode chorus in the magnetosphere. *J. Geophys. Res.* **122**, 675–694.
- 784 HSIEH, Y.-K. & OMURA, Y. 2017 Study of wave-particle interactions for whistler mode waves at
785 oblique angles by utilizing the gyroaveraging method. *Radio Science* **52** (10), 1268–1281,
786 2017RS006245.

- 787 ISLIKER, H., VLAHOS, L. & CONSTANTINESCU, D. 2017 Fractional Transport in Strongly
788 Turbulent Plasmas. *Phys. Rev. Lett.* **119** (4), 045101, arXiv: 1707.01526.
- 789 ITIN, A. P. & NEISHTADT, A. I. 2012 Fermi acceleration in time-dependent rectangular billiards
790 due to multiple passages through resonances. *Chaos* **22** (2), 026119, arXiv: 1112.3472.
- 791 ITIN, A. P., NEISHTADT, A. I. & VASILIEV, A. A. 2000 Captures into resonance and
792 scattering on resonance in dynamics of a charged relativistic particle in magnetic field
793 and electrostatic wave. *Physica D: Nonlinear Phenomena* **141**, 281–296.
- 794 KARIMABADI, H., AKIMOTO, K., OMIDI, N. & MENYUK, C. R. 1990 Particle acceleration by a
795 wave in a strong magnetic field - Regular and stochastic motion. *Physics of Fluids B* **2**,
796 606–628.
- 797 KARPMAN, V. I. 1974 Nonlinear Effects in the ELF Waves Propagating along the Magnetic
798 Field in the Magnetosphere. *Space Sci. Rev.* **16**, 361–388.
- 799 KATOH, Y. 2014 A simulation study of the propagation of whistler-mode chorus in the Earth's
800 inner magnetosphere. *Earth, Planets, and Space* **66**, 6.
- 801 KATOH, Y. & OMURA, Y. 2011 Amplitude dependence of frequency sweep rates of whistler
802 mode chorus emissions. *J. Geophys. Res.* **116**, 7201.
- 803 KATOH, Y. & OMURA, Y. 2013 Effect of the background magnetic field inhomogeneity on
804 generation processes of whistler-mode chorus and broadband hiss-like emissions. *J.*
805 *Geophys. Res.* **118**, 4189–4198.
- 806 KATOH, Y. & OMURA, Y. 2016 Electron hybrid code simulation of whistler-mode chorus
807 generation with real parameters in the Earth's inner magnetosphere. *Earth, Planets, and*
808 *Space* **68** (1), 192.
- 809 KENNEL, C. F. & ENGELMANN, F. 1966 Velocity Space Diffusion from Weak Plasma Turbulence
810 in a Magnetic Field. *Physics of Fluids* **9**, 2377–2388.
- 811 KERSTEN, T., HORNE, R. B., GLAUERT, S. A., MEREDITH, N. P., FRASER, B. J. & GREW,
812 R. S. 2014 Electron losses from the radiation belts caused by EMIC waves. *J. Geophys.*
813 *Res.* **119**, 8820–8837.
- 814 KHAZANOV, G. V., TEL'NIKHIN, A. A. & KRONBERG, T. K. 2013 Radiation belt electron
815 dynamics driven by large-amplitude whistlers. *Journal of Geophysical Research (Space*
816 *Physics)* **118** (10), 6397–6404.
- 817 KHAZANOV, G. V., TEL'NIKHIN, A. A. & KRONBERG, T. K. 2014 Stochastic electron motion
818 driven by space plasma waves. *Nonlinear Processes in Geophysics* **21** (1), 61–85.
- 819 KITAHARA, M. & KATOH, Y. 2019 Anomalous Trapping of Low Pitch Angle Electrons by
820 Coherent Whistler Mode Waves. *J. Geophys. Res.* **124** (7), 5568–5583.
- 821 KLETZING, C. A., KURTH, W. S., ACUNA, M., MACDOWALL, R. J., TORBERT, R. B.,
822 AVERKAMP, T., BODET, D., BOUNDS, S. R., CHUTTER, M., CONNERNEY, J., CRAWFORD,
823 D., DOLAN, J. S., DVORSKY, R., HOSPODARSKY, G. B., HOWARD, J., JORDANOVA,
824 V., JOHNSON, R. A., KIRCHNER, D. L., MOKRZYCKI, B., NEEDELL, G., ODOM, J.,
825 MARK, D., PFAFF, R., PHILLIPS, J. R., PIKER, C. W., REMINGTON, S. L., ROWLAND,
826 D., SANTOLIK, O., SCHNURR, R., SHEPPARD, D., SMITH, C. W., THORNE, R. M. &
827 TYLER, J. 2013 The Electric and Magnetic Field Instrument Suite and Integrated Science
828 (EMFISIS) on RBSP. *Space Sci. Rev.* **179**, 127–181.
- 829 KRAFFT, C. & VOLOKITIN, A. S. 2016 Electron Acceleration by Langmuir Waves Produced by
830 a Decay Cascade. *Astrophys. J.* **821**, 99.
- 831 KRAFFT, C., VOLOKITIN, A. S. & KRASNOSELSKIKH, V. V. 2013 Interaction of Energetic
832 Particles with Waves in Strongly Inhomogeneous Solar Wind Plasmas. *Astrophys. J.*
833 **778**, 111.
- 834 KUBOTA, Y. & OMURA, Y. 2017 Rapid precipitation of radiation belt electrons induced by
835 EMIC rising tone emissions localized in longitude inside and outside the plasmopause.
836 *Journal of Geophysical Research (Space Physics)* **122** (1), 293–309.
- 837 KUBOTA, Y. & OMURA, Y. 2018 Nonlinear Dynamics of Radiation Belt Electrons Interacting
838 With Chorus Emissions Localized in Longitude. *Journal of Geophysical Research (Space*
839 *Physics)* **123**, 4835–4857.
- 840 KUBOTA, Y., OMURA, Y. & SUMMERS, D. 2015 Relativistic electron precipitation induced by
841 EMIC-triggered emissions in a dipole magnetosphere. *Journal of Geophysical Research*
842 *(Space Physics)* **120** (6), 4384–4399.
- 843 KUZICHEV, I. V., VASKO, I. Y., RUALDO SOTO-CHAVEZ, A., TONG, Y., ARTEMYEV, A. V.,

- 844 BALE, S. D. & SPITKOVSKY, A. 2019 Nonlinear Evolution of the Whistler Heat Flux
845 Instability. *Astrophys. J.* **882** (2), 81, arXiv: 1907.04878.
- 846 LE QUEAU, D. & ROUX, A. 1987 Quasi-monochromatic wave-particle interactions in
847 magnetospheric plasmas. *Solar Physics* **111**, 59–80.
- 848 LEONCINI, X., VASILIEV, A. & ARTEMYEV, A. 2018 Resonance controlled transport in phase
849 space. *Physica D Nonlinear Phenomena* **364**, 22–26.
- 850 LERCHE, I. 1968 Quasilinear Theory of Resonant Diffusion in a Magneto-Active, Relativistic
851 Plasma. *Physica of Fluids* **11**.
- 852 LI, W., SANTOLIK, O., BORTNIK, J., THORNE, R. M., KLETZING, C. A., KURTH, W. S. &
853 HOSPODARSKY, G. B. 2016 New chorus wave properties near the equator from Van Allen
854 Probes wave observations. *Geophys. Res. Lett.* **43**, 4725–4735.
- 855 LI, W., THORNE, R. M., MA, Q., NI, B., BORTNIK, J., BAKER, D. N., SPENCE, H. E.,
856 REEVES, G. D., KANEKAL, S. G., GREEN, J. C., KLETZING, C. A., KURTH, W. S.,
857 HOSPODARSKY, G. B., BLAKE, J. B., FENNELL, J. F. & CLAUDEPIERRE, S. G. 2014
858 Radiation belt electron acceleration by chorus waves during the 17 March 2013 storm.
859 *J. Geophys. Res.* **119**, 4681–4693.
- 860 LICHTENBERG, A. J. & LIEBERMAN, M. A. 1983 *Regular and stochastic motion*.
- 861 LUNDIN, B. V. & SHKLIAR, D. R. 1977 Interaction of electrons with low transverse velocities
862 with VLF waves in an inhomogeneous plasma. *Geomagnetism and Aeronomy* **17**, 246–251.
- 863 LYONS, L. R. & WILLIAMS, D. J. 1984 *Quantitative aspects of magnetospheric physics..*
- 864 MA, Q., LI, W., BORTNIK, J., THORNE, R. M., CHU, X., OZEKE, L. G., REEVES, G. D.,
865 KLETZING, C. A., KURTH, W. S., HOSPODARSKY, G. B., ENGBRETSON, M. J., SPENCE,
866 H. E., BAKER, D. N., BLAKE, J. B., FENNELL, J. F. & CLAUDEPIERRE, S. G. 2018
867 Quantitative Evaluation of Radial Diffusion and Local Acceleration Processes During
868 GEM Challenge Events. *Journal of Geophysical Research (Space Physics)* **123** (3), 1938–
869 1952.
- 870 MA, Q., LI, W., THORNE, R. M., NISHIMURA, Y., ZHANG, X.-J., REEVES, G. D., KLETZING,
871 C. A., KURTH, W. S., HOSPODARSKY, G. B., HENDERSON, M. G., SPENCE, H. E.,
872 BAKER, D. N., BLAKE, J. B., FENNELL, J. F. & ANGELOPOULOS, V. 2016 Simulation
873 of energy-dependent electron diffusion processes in the Earth’s outer radiation belt. *J.*
874 *Geophys. Res.* **121**, 4217–4231.
- 875 MA, Q., MOURENAS, D., LI, W., ARTEMYEV, A. & THORNE, R. M. 2017 VLF waves from
876 ground-based transmitters observed by the Van Allen Probes: Statistical model and effects
877 on plasmaspheric electrons. *Geophys. Res. Lett.* **44**, 6483–6491.
- 878 MAUK, B. H., FOX, N. J., KANEKAL, S. G., KESSEL, R. L., SIBECK, D. G. & UKHORSKIY,
879 A. 2013 Science Objectives and Rationale for the Radiation Belt Storm Probes Mission.
880 *Space Sci. Rev.* **179**, 3–27.
- 881 MAUK, B. H., HAGGERTY, D. K., PARANICAS, C., CLARK, G., KOLLMANN, P., RYMER, A. M.,
882 BOLTON, S. J., LEVIN, S. M., ADRIANI, A., ALLEGRI, F., BAGENAL, F., BONFOND, B.,
883 CONNERNEY, J. E. P., GLADSTONE, G. R., KURTH, W. S., MCCOMAS, D. J. & VALEK,
884 P. 2017 Discrete and broadband electron acceleration in Jupiter’s powerful aurora. *Nature*
885 **549** (7670), 66–69.
- 886 MEANS, J. D. 1972 Use of the three-dimensional covariance matrix in analyzing the polarization
887 properties of plane waves. *J. Geophys. Res.* **77**, 5551.
- 888 MENIETTI, J. D., SHPRITS, Y. Y., HORNE, R. B., WOODFIELD, E. E., HOSPODARSKY, G. B.
889 & GURNETT, D. A. 2012 Chorus, ECH, and Z mode emissions observed at Jupiter and
890 Saturn and possible electron acceleration. *J. Geophys. Res.* **117**, A12214.
- 891 MEREDITH, N. P., HORNE, R. B., GLAUERT, S. A. & ANDERSON, R. R. 2007 Slot region
892 electron loss timescales due to plasmaspheric hiss and lightning-generated whistlers. *J.*
893 *Geophys. Res.* **112**, 8214.
- 894 MILLAN, R. M. & THORNE, R. M. 2007 Review of radiation belt relativistic electron losses.
895 *Journal of Atmospheric and Solar-Terrestrial Physics* **69**, 362–377.
- 896 MODENA, A., NAJMUDIN, Z., DANGOR, A. E., CLAYTON, C. E., MARSH, K. A., JOSHI, C.,
897 MALKA, V., DARROW, C. B., DANSON, C., NEELY, D. & WALSH, F. N. 1995 Electron
898 acceleration from the breaking of relativistic plasma waves. *Nature* **377** (6550), 606–608.
- 899 MOURENAS, D., ARTEMYEV, A., AGAPITOV, O. & KRASNOSSELSKIKH, V. 2012 Acceleration of
900 radiation belts electrons by oblique chorus waves. *J. Geophys. Res.* **117**, 10212.

- 901 MOURENAS, D., ARTEMYEV, A. V., AGAPITOV, O. V., KRASNOSELSKIKH, V. & MOZER, F. S.
902 2015 Very oblique whistler generation by low-energy electron streams. *J. Geophys. Res.*
903 **120**, 3665–3683.
- 904 MOURENAS, D., ARTEMYEV, A. V., AGAPITOV, O. V., MOZER, F. S. & KRASNOSELSKIKH,
905 V. V. 2016*a* Equatorial electron loss by double resonance with oblique and parallel intense
906 chorus waves. *J. Geophys. Res.* **121**, 4498–4517.
- 907 MOURENAS, D., ARTEMYEV, A. V., MA, Q., AGAPITOV, O. V. & LI, W. 2016*b* Fast dropouts of
908 multi-MeV electrons due to combined effects of EMIC and whistler mode waves. *Geophys.*
909 *Res. Lett.* **43** (9), 4155–4163.
- 910 MOURENAS, D., ZHANG, X.-J., ARTEMYEV, A. V., ANGELOPOULOS, V., THORNE, R. M.,
911 BORTNIK, J., NEISHTADT, A. I. & VASILIEV, A. A. 2018 Electron Nonlinear Resonant
912 Interaction With Short and Intense Parallel Chorus Wave Packets. *J. Geophys. Res.*
913 **123**, 4979–4999.
- 914 NEISHTADT, A. I. 1999 On Adiabatic Invariance in Two-Frequency Systems. in *Hamiltonian*
915 *Systems with Three or More Degrees of Freedom*, ed. Simo C., NATO ASI Series C.
916 Dordrecht: Kluwer Acad. Publ. **533**, 193–213.
- 917 NEISHTADT, A. I. 2014 Averaging, passage through resonances, and capture into resonance in
918 two-frequency systems. *Russian Mathematical Surveys* **69** (5), 771.
- 919 NEISHTADT, A. I. & VASILIEV, A. A. 2006 Destruction of adiabatic invariance at resonances in
920 slow fast Hamiltonian systems. *Nuclear Instruments and Methods in Physics Research A*
921 **561**, 158–165, arXiv: arXiv:nlin/0511050.
- 922 NI, B., THORNE, R. M., ZHANG, X., BORTNIK, J., PU, Z., XIE, L., HU, Z.-J., HAN, D., SHI,
923 R., ZHOU, C. & GU, X. 2016 Origins of the Earth's Diffuse Auroral Precipitation. *Space*
924 *Sci. Rev.* **200**, 205–259.
- 925 NISHIMURA, Y., BORTNIK, J., LI, W., THORNE, R. M., LYONS, L. R., ANGELOPOULOS, V.,
926 MENDE, S. B., BONNELL, J. W., LE CONTEL, O., CULLY, C., ERGUN, R. & AUSTER,
927 U. 2010 Identifying the Driver of Pulsating Aurora. *Science* **330**, 81–84.
- 928 NUNN, D. 1986 A nonlinear theory of sideband stability in ducted whistler mode waves. *Plan.*
929 *Sp. Sci.* **34**, 429–451.
- 930 NUNN, D. & OMURA, Y. 2012 A computational and theoretical analysis of falling frequency
931 VLF emissions. *J. Geophys. Res.* **117**, 8228.
- 932 NUNN, D. & OMURA, Y. 2015 A computational and theoretical investigation of nonlinear wave-
933 particle interactions in oblique whistlers. *J. Geophys. Res.* **120**, 2890–2911.
- 934 NUNN, D., SANTOLIK, O., RYCROFT, M. & TRAKHTENGERTS, V. 2009 On the numerical
935 modelling of VLF chorus dynamical spectra. *Annales Geophysicae* **27**, 2341–2359.
- 936 OMURA, Y., FURUYA, N. & SUMMERS, D. 2007 Relativistic turning acceleration of resonant
937 electrons by coherent whistler mode waves in a dipole magnetic field. *J. Geophys. Res.*
938 **112**, 6236.
- 939 OMURA, Y., KATOH, Y. & SUMMERS, D. 2008 Theory and simulation of the generation of
940 whistler-mode chorus. *J. Geophys. Res.* **113**, 4223.
- 941 OMURA, Y., MATSUMOTO, H., NUNN, D. & RYCROFT, M. J. 1991 A review of observational,
942 theoretical and numerical studies of VLF triggered emissions. *Journal of Atmospheric and*
943 *Terrestrial Physics* **53**, 351–368.
- 944 OMURA, Y., MIYASHITA, Y., YOSHIKAWA, M., SUMMERS, D., HIKISHIMA, M., EBIHARA, Y. &
945 KUBOTA, Y. 2015 Formation process of relativistic electron flux through interaction with
946 chorus emissions in the Earth's inner magnetosphere. *J. Geophys. Res.* **120**, 9545–9562.
- 947 OMURA, Y., NUNN, D. & SUMMERS, D. 2013 Generation Processes of Whistler Mode Chorus
948 Emissions: Current Status of Nonlinear Wave Growth Theory. In *Dynamics of the Earth's*
949 *Radiation Belts and Inner Magnetosphere* (ed. D. Summers, I. U. Mann, D. N. Baker &
950 M. Schulz), pp. 243–254.
- 951 PALMADESSO, P. J. 1972 Resonance, Particle Trapping, and Landau Damping in Finite
952 Amplitude Obliquely Propagating Waves. *Physics of Fluids* **15**, 2006–2013.
- 953 ROBERG-CLARK, G. T., AGAPITOV, O., DRAKE, J. F. & SWISDAK, M. 2019 Scattering of
954 Energetic Electrons by Heat-flux-driven Whistlers in Flares. *Astrophys. J.* **887** (2), 190,
955 arXiv: 1908.06481.
- 956 RYUTOV, D. D. 1969 Quasilinear Relaxation of an Electron Beam in an Inhomogeneous Plasma.
957 *Soviet Journal of Experimental and Theoretical Physics* **30**, 131.

- 958 SAGDEEV, R. Z., USIKOV, D. A. & ZASLAVSKY, G. M. 1988 *Nonlinear Physics. From the*
959 *Pendulum to Turbulence and Chaos*.
- 960 SANTOLÍK, O., KLETZING, C. A., KURTH, W. S., HOSPODARSKY, G. B. & BOUNDS, S. R. 2014
961 Fine structure of large-amplitude chorus wave packets. *Geophys. Res. Lett.* **41**, 293–299.
- 962 SHAPIRO, V. D. & SAGDEEV, R. Z. 1997 Nonlinear wave-particle interaction and conditions for
963 the applicability of quasilinear theory. *Physics Reports* **283**, 49–71.
- 964 SHEELEY, B. W., MOLDWIN, M. B., RASSOUL, H. K. & ANDERSON, R. R. 2001 An empirical
965 plasmasphere and trough density model: CRRES observations. *J. Geophys. Res.* **106**,
966 25631–25642.
- 967 SHKLYAR, D. R. 1981 Stochastic motion of relativistic particles in the field of a monochromatic
968 wave. *Sov. Phys. JETP* **53**, 1197–1192.
- 969 SHKLYAR, D. R. 2011 On the nature of particle energization via resonant wave-particle
970 interaction in the inhomogeneous magnetospheric plasma. *Annales Geophysicae* **29**, 1179–
971 1188.
- 972 SHKLYAR, D. R. & MATSUMOTO, H. 2009 Oblique Whistler-Mode Waves in the Inhomogeneous
973 Magnetospheric Plasma: Resonant Interactions with Energetic Charged Particles. *Surveys*
974 *in Geophysics* **30**, 55–104.
- 975 SHKLYAR, D. R. & ZIMBARDO, G. 2014 Particle dynamics in the field of two waves in a
976 magnetoplasma. *Plasma Physics and Controlled Fusion* **56** (9), 095002.
- 977 SHPRITS, Y. Y., DROZDOV, A. Y., SPASOJEVIC, M., KELLERMAN, A. C., USANOVA, M. E.,
978 ENGBRETSON, M. J., AGAPITOV, O. V., ZHELAVSKAYA, I. S., RAITA, T. J., SPENCE,
979 H. E., BAKER, D. N., ZHU, H. & ASEEV, N. A. 2016 Wave-induced loss of ultra-
980 relativistic electrons in the Van Allen radiation belts. *Nature Communications* **7**, 12883.
- 981 SHPRITS, Y. Y., SUBBOTIN, D. A., MEREDITH, N. P. & ELKINGTON, S. R. 2008 Review of
982 modeling of losses and sources of relativistic electrons in the outer radiation belt II: Local
983 acceleration and loss. *Journal of Atmospheric and Solar-Terrestrial Physics* **70**, 1694–
984 1713.
- 985 SILIN, I., MANN, I. R., SYDORA, R. D., SUMMERS, D. & MACE, R. L. 2011 Warm plasma effects
986 on electromagnetic ion cyclotron wave MeV electron interactions in the magnetosphere.
987 *Journal of Geophysical Research (Space Physics)* **116** (A5), A05215.
- 988 SOLOVEV, V. V. & SHKLIAR, D. R. 1986 Particle heating by a low-amplitude wave in an
989 inhomogeneous magnetoplasma. *Sov. Phys. JETP* **63**, 272–277.
- 990 STIX, T. H. 1962 *The Theory of Plasma Waves*.
- 991 SUMMERS, D., OMURA, Y., NAKAMURA, S. & KLETZING, C. A. 2014 Fine structure of
992 plasmaspheric hiss. *J. Geophys. Res.* **119**, 9134–9149.
- 993 SUMMERS, D. & THORNE, R. M. 2003 Relativistic electron pitch-angle scattering by
994 electromagnetic ion cyclotron waves during geomagnetic storms. *J. Geophys. Res.* **108**,
995 1143.
- 996 SUMMERS, D., THORNE, R. M. & XIAO, F. 1998 Relativistic theory of wave-particle resonant
997 diffusion with application to electron acceleration in the magnetosphere. *J. Geophys.*
998 *Res.* **103**, 20487–20500.
- 999 TAO, X. 2014 A numerical study of chorus generation and the related variation of wave intensity
1000 using the DAWN code. *Journal of Geophysical Research (Space Physics)* **119** (5), 3362–
1001 3372.
- 1002 TAO, X. & BORTNIK, J. 2010 Nonlinear interactions between relativistic radiation belt electrons
1003 and oblique whistler mode waves. *Nonlinear Processes in Geophysics* **17**, 599–604.
- 1004 TAO, X., BORTNIK, J., ALBERT, J. M. & THORNE, R. M. 2012a Comparison of bounce-averaged
1005 quasi-linear diffusion coefficients for parallel propagating whistler mode waves with test
1006 particle simulations. *J. Geophys. Res.* **117**, 10205.
- 1007 TAO, X., BORTNIK, J., ALBERT, J. M., THORNE, R. M. & LI, W. 2013 The importance of
1008 amplitude modulation in nonlinear interactions between electrons and large amplitude
1009 whistler waves. *Journal of Atmospheric and Solar-Terrestrial Physics* **99**, 67–72.
- 1010 TAO, X., LI, W., BORTNIK, J., THORNE, R. M. & ANGELOPOULOS, V. 2012b Comparison
1011 between theory and observation of the frequency sweep rates of equatorial rising tone
1012 chorus. *Geophys. Res. Lett.* **39** (8), L08106.
- 1013 TAO, X., ZONCA, F. & CHEN, L. 2017 Identify the nonlinear wave-particle interaction regime
1014 in rising tone chorus generation. *Geophys. Res. Lett.* **44** (8), 3441–3446.

- 1015 TAO, X., ZONCA, F., CHEN, L. & WU, Y. 2020 Theoretical and numerical studies of chorus
1016 waves: A review. *Science China Earth Sciences* **63** (1), 78–92.
- 1017 THORNE, R. M. 2010 Radiation belt dynamics: The importance of wave-particle interactions.
1018 *Geophys. Res. Lett.* **37**(2), 22107.
- 1019 THORNE, R. M. & KENNEL, C. F. 1971 Relativistic electron precipitation during magnetic
1020 storm main phase. *J. Geophys. Res.* **76**, 4446.
- 1021 THORNE, R. M., LI, W., NI, B., MA, Q., BORTNIK, J., CHEN, L., BAKER, D. N., SPENCE,
1022 H. E., REEVES, G. D., HENDERSON, M. G., KLETZING, C. A., KURTH, W. S.,
1023 HOSPODARSKY, G. B., BLAKE, J. B., FENNEL, J. F., CLAUDEPIERRE, S. G. &
1024 KANEKAL, S. G. 2013 Rapid local acceleration of relativistic radiation-belt electrons by
1025 magnetospheric chorus. *Nature* **504**, 411–414.
- 1026 THORNE, R. M., NI, B., TAO, X., HORNE, R. B. & MEREDITH, N. P. 2010 Scattering by chorus
1027 waves as the dominant cause of diffuse auroral precipitation. *Nature* **467**, 943–946.
- 1028 TIKHONCHUK, V. T. 2019 Physics of laser plasma interaction and particle transport in the
1029 context of inertial confinement fusion. *Nuclear Fusion* **59** (3), 032001.
- 1030 TITOVA, E. E., KOZELOV, B. V., JIRICEK, F., SMILAUER, J., DEMEKHOV, A. G. &
1031 TRAKHTENGERTS, V. Y. 2003 Verification of the backward wave oscillator model of VLF
1032 chorus generation using data from MAGION 5 satellite. *Annales Geophysicae* **21**, 1073–
1033 1081.
- 1034 TONG, Y., VASKO, I. Y., ARTEMYEV, A. V., BALE, S. D. & MOZER, F. S. 2019 Statistical
1035 Study of Whistler Waves in the Solar Wind at 1 au. *Astrophys. J.* **878** (1), 41, arXiv:
1036 1905.08958.
- 1037 TYLER, E., BRENNEMAN, A., CATTELL, C., WYGANT, J., THALLER, S. & MALASPINA, D. 2019
1038 Statistical Occurrence and Distribution of High-Amplitude Whistler Mode Waves in the
1039 Outer Radiation Belt. *Geophys. Res. Lett.* **46** (5), 2328–2336.
- 1040 VAINCHTEIN, D., ZHANG, X.-J., ARTEMYEV, A., MOURENAS, D., ANGELOPOULOS, V. &
1041 THORNE, R. M. 2018 Evolution of electron distribution driven by nonlinear resonances
1042 with intense field-aligned chorus waves. *J. Geophys. Res.* .
- 1043 VAN KAMPEN, N. G. 2003 *Stochastic Processes in Physics and Chemistry*, 3rd edn. North
1044 Holland.
- 1045 VASILEV, A. A., ZASLAVSKII, G. M., NATENZON, M. I., NEISHTADT, A. I. & PETROVICHEV,
1046 B. A. 1988 Attractors and stochastic attractors of motion in a magnetic field. *Zhurnal*
1047 *Ekspierimentalnoi i Teoreticheskoi Fiziki* **94**, 170–187.
- 1048 VEDENOV, A. A., VELIKHOV, E. & SAGDEEV, R. 1962 Quasilinear theory of plasma oscillations.
1049 *Nuclear Fusion Suppl.* **2**, 465–475.
- 1050 WANG, R., VASKO, I. Y., MOZER, F. S., BALE, S. D., ARTEMYEV, A. V., BONNELL, J. W.,
1051 ERGUN, R., GILES, B., LINDQVIST, P. A., RUSSELL, C. T. & STRANGWAY, R. 2020
1052 Electrostatic Turbulence and Debye-scale Structures in Collisionless Shocks. *Astrophys.*
1053 *J. Lett.* **889** (1), L9, arXiv: 1912.01770.
- 1054 WATT, C. E. J. & RANKIN, R. 2009 Electron Trapping in Shear Alfvén Waves that Power the
1055 Aurora. *Physical Review Letters* **102** (4), 045002.
- 1056 WILSON, L. B., KOVAL, A., SZABO, A., BRENNEMAN, A., CATTELL, C. A., GOETZ, K.,
1057 KELLOGG, P. J., KERSTEN, K., KASPER, J. C., MARUCA, B. A. & PULUPA, M.
1058 2013 Electromagnetic waves and electron anisotropies downstream of supercritical
1059 interplanetary shocks. *J. Geophys. Res.* **118**, 5–16, arXiv: 1207.6429.
- 1060 WILSON, III, L. B., CATTELL, C., KELLOGG, P. J., GOETZ, K., KERSTEN, K., HANSON,
1061 L., MACGREGOR, R. & KASPER, J. C. 2007 Waves in Interplanetary Shocks: A
1062 Wind/WAVES Study. *Physical Review Letters* **99** (4), 041101.
- 1063 WILSON, III, L. B., CATTELL, C. A., KELLOGG, P. J., WYGANT, J. R., GOETZ, K.,
1064 BRENNEMAN, A. & KERSTEN, K. 2011 The properties of large amplitude whistler mode
1065 waves in the magnetosphere: Propagation and relationship with geomagnetic activity.
1066 *Geophys. Res. Lett.* **38**, 17107.
- 1067 WILSON, III, L. B., KOVAL, A., SZABO, A., BRENNEMAN, A., CATTELL, C. A., GOETZ, K.,
1068 KELLOGG, P. J., KERSTEN, K., KASPER, J. C., MARUCA, B. A. & PULUPA, M. 2012
1069 Observations of electromagnetic whistler precursors at supercritical interplanetary shocks.
1070 *Geophys. Res. Lett.* **39**, 8109.

- 1071 YOON, P. H., SEOUGH, J., SALEM, C. S. & KLEIN, K. G. 2019 Solar Wind Temperature
1072 Isotropy. *Phys. Rev. Lett.* **123** (14), 145101.
- 1073 YU, J., WANG, J., LI, L. Y., CUI, J., CAO, J. B. & HE, Z. G. 2020 Electron diffusion
1074 by coexisting plasmaspheric hiss and chorus waves: Multisatellite observations and
1075 simulations. *Geophysical Research Letters* **47** (15), e2020GL088753.
- 1076 ZASLAVSKII, G. M., ZAKHAROV, M. I., NEISHTADT, A. I., SAGDEEV, R. Z. & USIKOV, D. A.
1077 1989 Multidimensional Hamiltonian chaos. *Zhurnal Eksperimentalnoi i Teoreticheskoi*
1078 *Fiziki* **96**, 1563–1586.
- 1079 ZASLAVSKY, A., KRAFFT, C., GORBUNOV, L. & VOLOKITIN, A. 2008 Wave-particle interaction
1080 at double resonance. *Phys. Rev. E* **77** (5), 056407.
- 1081 ZASLAVSKY, G. M. 2005 *Hamiltonian Chaos and Fractional Dynamics*. Oxford: Oxford
1082 University Press.
- 1083 ZELENYI, L. M. & MILOVANOV, A. V. 2004 Fractal topology and strange kinetics: from
1084 percolation theory to problems in cosmic electrodynamics. *Physics Uspekhi* **47**, 749–788.
- 1085 ZHANG, X. J., AGAPITOV, O., ARTEMYEV, A. V., MOURENAS, D., ANGELOPOULOS, V.,
1086 KURTH, W. S., BONNELL, J. W. & HOSPODARSKY, G. B. 2020a Phase Decoherence
1087 Within Intense Chorus Wave Packets Constrains the Efficiency of Nonlinear Resonant
1088 Electron Acceleration. *Geophys. Res. Lett.* **47** (20), e89807.
- 1089 ZHANG, X.-J., LI, W., THORNE, R. M., ANGELOPOULOS, V., BORTNIK, J., KLETZING, C. A.,
1090 KURTH, W. S. & HOSPODARSKY, G. B. 2016 Statistical distribution of EMIC wave
1091 spectra: Observations from Van Allen Probes. *Geophys. Res. Lett.* **43**, 12.
- 1092 ZHANG, X. J., MOURENAS, D., ARTEMYEV, A. V., ANGELOPOULOS, V., BORTNIK, J., THORNE,
1093 R. M., KURTH, W. S., KLETZING, C. A. & HOSPODARSKY, G. B. 2019 Nonlinear Electron
1094 Interaction With Intense Chorus Waves: Statistics of Occurrence Rates. *Geophys. Res.*
1095 *Lett.* **46** (13), 7182–7190.
- 1096 ZHANG, X. J., MOURENAS, D., ARTEMYEV, A. V., ANGELOPOULOS, V., KURTH, W. S.,
1097 KLETZING, C. A. & HOSPODARSKY, G. B. 2020b Rapid Frequency Variations Within
1098 Intense Chorus Wave Packets. *Geophys. Res. Lett.* **47** (15), e88853.
- 1099 ZHANG, X.-J., MOURENAS, D., ARTEMYEV, A. V., ANGELOPOULOS, V. & THORNE, R. M.
1100 2017 Contemporaneous EMIC and whistler mode waves: Observations and consequences
1101 for MeV electron loss. *Geophys. Res. Lett.* **44**, 8113–8121.
- 1102 ZHANG, X. J., THORNE, R., ARTEMYEV, A., MOURENAS, D., ANGELOPOULOS, V., BORTNIK,
1103 J., KLETZING, C. A., KURTH, W. S. & HOSPODARSKY, G. B. 2018 Properties of
1104 Intense Field-Aligned Lower-Band Chorus Waves: Implications for Nonlinear Wave-
1105 Particle Interactions. *Journal of Geophysical Research (Space Physics)* **123** (7), 5379–
1106 5393.
- 1107 ZHENG, L., CHEN, L. & ZHU, H. 2019 Modeling Energetic Electron Nonlinear Wave-Particle
1108 Interactions With Electromagnetic Ion Cyclotron Waves. *Journal of Geophysical Research*
1109 *(Space Physics)* **124** (5), 3436–3453.